iScience

CellPress
OPEN ACCESS

Review

# Designable structural coloration by colloidal particle assembly: from nature to artificial manufacturing

Kaixuan Li,[1,2] Chang Li,[1] Huizeng Li,[1] Mingzhu Li,[1,3,*] and Yanlin Song[1,2,*]

## SUMMARY

**Structural color attracts considerable scientific interests and industrial explorations in various fields for the eco-friendly, fade-resistant, and dynamic advantages. After the long-period evolution, nature has achieved the optimized color structures at various length scales, which has inspired people to learn and replicate them to improve the artificial structure color. In this review, we focus on the design of artificial structural colors based on colloidal particle assembly and summarize the functional bioinspired structure colors. We demonstrate the design principles of biomimetic structural colors via the precise structure engineering and typical bottom-up methods. Some main applications are outlined in the following chapter. Finally, we propose the existing challenges and promising prospects. This review is expected to introduce the recent design strategies about the artificial structure colors and provide the insights for its future development.**

## INTRODUCTION

Color is an indispensable part of our human society. It not only decorates the beautiful world but also plays an important role in display (Daqiqeh Rezaei et al., 2020), information (Hong et al., 2020), and medical applications (Lee et al., 2018). The generation of color is perceived from the light interactions with specific matters, such as absorption, reflection, refraction, scattering, diffraction, and so on (Kristensen et al., 2016). According to the different sources, colors can be divided into pigmentary colors and structural colors. Pigmentary colors are realized by the color molecules (all dyes and most pigments), which can absorb light within a definite range of wavelengths but reflect and/or refract the non-absorbed light to manifest color (Kulyk et al., 2020). In contrast, structural colors result from the physical micro- or nanostructures at the scale of visible wavelengths (Ren et al., 2019). Compared with the pigmentary colors, structural colors can resist to the photobleaching and avoid the use of toxic dyes. Thus, they can be eco-friendly and fade-resistant, which make them promising candidates for the future color applications (Hou et al., 2018).

Structural colors are commonly found in nature. Through long-time evolution and natural selection, they have been a glorious feature of natural creatures (Watanabe et al., 2004; Zi et al., 2003). Plants can exhibit an incredible variety of structural colors, which are skillfully exploited not only to interact with their environment (i.e., attract pollinators) (Whitney et al., 2009), but also to harvest energy from sunlight (Tadepalli et al., 2017). For animals, the structural colors contribute a lot to the information communications including camouflage, reproduction, and signal transmission (Shang et al., 2019). Taking the chameleons as an example, the skin can exhibit complex and rapid color changes with the surrounding environment to protect them from harm (Wang et al., 2019a). Another fascinating property of natural structure color is that the vivid colors are prepared with the very common materials. The excellent optical properties are achieved by the extraordinarily precise engineering to optimize the structure at various length scales (Li et al., 2020; Zhao et al., 2012). These outstanding features have attracted much research effort in material science, chemistry, engineering and physics, and inspired scientists to study the biomimetic structures (Liu and Jiang, 2011). Accordingly, various artificial structural-color materials are fabricated by duplicating or mimicking the components existing in natural creatures (Goerlitzer et al., 2018; Kolle et al., 2013). These artificial structural colors can be non-iridescent (Xiao et al., 2017), brilliant, and responsive to various external stimuli including the temperature, solvent, light, electricity, magnetic field, and forces (Fenzl et al., 2014), which make them promising in many applications, such as colorful displays, anti-counterfeiting, information storage, mechanical sensing, and healthcare monitoring (Isapour and Lattuada,

[1]Key Laboratory of Green Printing, CAS Research/Education Center for Excellence in Molecular Sciences, Institute of Chemistry, Chinese Academy of Sciences, Beijing 100190, P. R. China

[2]University of Chinese Academy of Sciences, Beijing 100049, P. R. China

[3]Key Laboratory of Materials Processing and Mold of the Ministry of Education, National Engineering Research Center for Advanced Polymer Processing Technology, Zhengzhou University, Zhengzhou 450002, P. R. China

*Correspondence: mingzhu@iccas.ac.cn (M.L.), ylsong@iccas.ac.cn (Y.S.)

https://doi.org/10.1016/j.isci.2021.102121

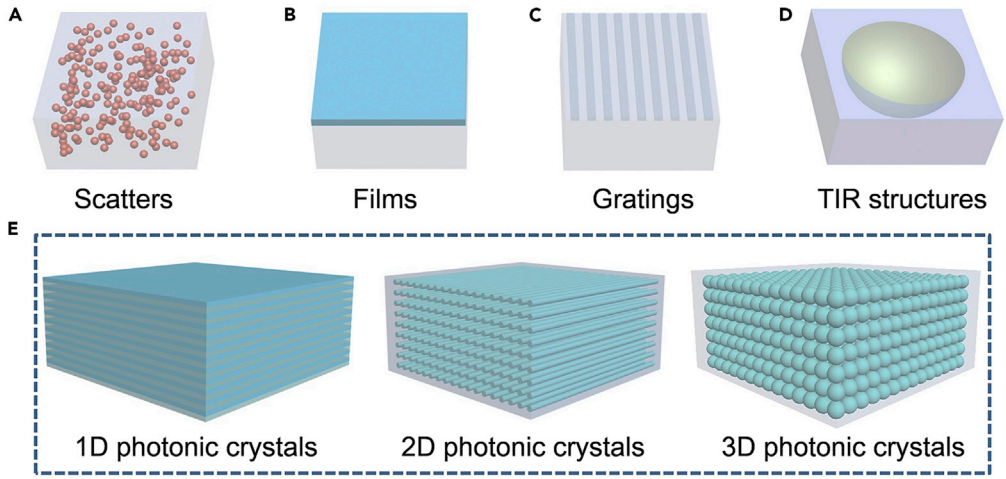


**Figure 1. The basic color structures of different scales**

(A) Scatters composed of the small particles with disordered arrangement.

(B) Thin-film structures by depositing materials on a substrate.

(C) Diffraction gratings with periodic patterns on the substrate surface.

(D) Total internal reflection structures composed of the microscale concave interface.

(E) One-, two- and three-dimensional (1D, 2D and 3D) photonic crystals with a structural periodicity in one, two, or three directions, respectively.

2018). With the in-depth understanding of the color mechanisms, researchers have already obtained the optimization of some artificial structural colors aiming at the specific functions (Wu et al., 2020). Thus, more advanced structural-color materials and products are expected to be prepared and applied in the future.

In this review, we put an emphasis on the bioinspired structural colors by colloidal particle assembly, as follows: First, we give a brief overview of the basic color structures of different scales and demonstrate the coloration mechanisms. Next, we summarize the functional structure-color designs with different properties. Aiming at functions, the techniques to manufacture the artificial structural color are described. Some typical applications are listed in the following. Finally, we propose the challenges and opportunities associated with the artificial structure colors.

## BASIC COLOR STRUCTURES OF DIFFERENT SCALES

The generation of structural color is resulted from light interactions with the specific micro- or nanostructures (Ji et al., 2017). Over the natural evolution of millions years, biological systems have developed multiscale well-controlled structures (Zhang et al., 2016). For the similar sizes with visible wavelengths between 400 and 700 nm, these microstructures can display vivid colors by the interactions with light (Sun et al., 2013), which provide the design criteria for artificial structural colors (Kinoshita et al., 2008). According to the different scales, we have summarized the basic chromogenic structures.

### Scatters

Light scattering depicts the light interactions with elementary particles of matter (scatterers) (Skipetrov and Sokolov, 2014). The size for small scatters can be below the wavelength and in the scale of a few nanometers. Commonly, the blue color in the sky is generated by the scattering effect. Divided by the different coloration mechanisms, scattering can be simply classified into the coherent scattering and the incoherent scattering. For the coherent scattering, scatterers are arranged in relative order (Sköld et al., 1972). There exists a phase relationship between the scattered lights. Thus, the scattered lights can interact with each other and the colors by coherent scattering can display iridescent property. In contrast, the disordered dispersion of scatterers leads to the incoherent scattering. As shown in Figure 1A, it has a diffuse reflection, with the spectrum unrelated to the observation or the illumination angles. According to the scatterer morphology, it is called Mie scattering when the scatterers are spherical particles. When the size of small scatters is well below the wavelength, it is the Rayleigh scattering. Rayleigh scattering is a typical incoherent scattering. The

molecules within the atmosphere by Rayleigh scattering cause the blue color of the sky. The white appearance in clouds and the red color in sunset are also caused by the Rayleigh scattering (Young, 1981).

### Films

Interference in nature involves the single-layer film interference and multilayer film interference (Pancharatnam, 1956). Typically, the glaring color of soap bubble is caused by the thin-film interference. The general geometry of light interacting with a thin film is schematically illustrated in Figure 1B. The key factors generating the interference are the layered media composed of the film and surrounding media with different refractive indexes. For a given angle and wavelength of incident light, the interference will happen between the light waves reflected from the upper and lower interfaces of the film. Multi-film interference results from the periodic stack of a pair of thin layers, which can manipulate the multiple reflections at the interfaces and therefore further enhance interference effects. Colors produced by the multi-film interference are brighter, more colorful and saturated. They widely exit in many organisms, such as insects, birds, fish, mollusks, and fruits (Vukusic and Sambles, 2003). The interference color highly depends on the refracting angles, which means the observed color will change at different viewing conditions. Hence, this structural color often presents the typical iridescent features.

### Gratings

Diffraction gratings are periodic structures that can split and diffract light into several beams traveling in different directions, which can induce the structural color (Loewen and Popov, 2018). The color is regulated by the spacing between the neighboring structures, as well as the direction of observation (Yang et al., 2020). Usually, the diffraction grating is fabricated by surface-patterning of subwavelength periodical stripes with a typical spacing $d$ (Figure 1C). When a beam of light irradiates the grating surface at an incident angle of $\theta_i$, and is diffracted at an angle of $\theta_r$, the wavelength of the corresponding diffracted light can be calculated as,

$$M\,\lambda = d\,(\sin\theta i - \sin\theta r) \qquad \text{(Equation 1)}$$

here $m$ is the diffraction order (an integer). Both $\theta_i$ and $\theta_r$ are the directions from the normal of the reflective plane. The diffraction grating is an important tool in scientific research and technology. Structural coloration by the diffraction grating is common in nature (*e.g* flower, butterfly, and shells) (Kinoshita and Yoshioka, 2005). Some of them have been applied in daily life (*e.g* the compact disc, anti-fake labels, and beautiful decorations) (Botten et al., 1981).

### Photonic crystals

In the late 1980s, the modern field of photonic crystals (PCs) was born. PCs are a kind of periodic dielectric structures with the ability to manipulate photons (Joannopoulos et al., 1997). Biological systems contain many different examples of PCs with refractive index periodicities including the 1D geometry of multilayer systems, 2D, and 3D arrangements (Figure 1E). The photonic bandgap (PBG) is formed by creating the periodic structure units with alternating refractive indices, which can block the propagation of electromagnetic radiation (Foresi et al., 1997). By modulating the period of the PCs, the propagation of light with certain wavelengths can be forbidden. When the periodicities of the PCs are on the order of the wavelength of visible light, the specific light is reflected, which can result in the vivid structure colors. The PC-based structural colors can be made from many materials (López, 2003). Importantly, the assembly of colloidal PCs with mono-dispersed colloidal microspheres into face-centered cubic (FCC) structures has been a popular way to crate the structural color for the economic and large-area processing (Moon and Yang, 2010). Colloidal spheres are able to be obtained from inorganic silica and organic polymer materials. By adjusting the diameter of colloidal spheres and assembly conditions, the PC-based structural colors are easy to be prepared and regulated (Aguirre et al., 2010; Ge et al., 2007).

### Total internal reflection structures

The total internal reflection (TIR) usually happens in spherical structures on the range of a few microns to hundred microns (Figure 1D), such as the raindrop, multiphase droplets, and concave interfaces, which can induce the refraction splitting the white light into the colorful light with specific wavelength (Zhu et al., 1986). The colors of the rainbow are the typical example resulted from the TIR (Nussenzveig, 1969). Recently, Goodling et al. demonstrated a new coloration mechanism based on the TIR and interference mechanism that light traveling along different trajectories of TIR at a concave optical interface was

able to interfere to generate the brilliant structure color (Goodling et al., 2019). The color could be manipulated by controlling the interface morphology including the size and contact angle. Due to the TIR in the concave microcavity of the butterfly *Papilio blumei*, the phenomena of color mixing and polarization conversion are found (Kolle et al., 2010). The fabrication of TIR-based structures is simple and efficient, which can add more vitality to structural colors.

In addition to the mentioned chromogenic structures, the colors in natural creatures can also be created by the hierarchical structures (Chen et al., 2020). For the optimally designed and tightly regulated structures, natural systems demonstrate an exquisite control over the light-matter interactions at various length scales, which enables them enhance or modify their functions with the limited materials (Shin et al., 2003). Some special color features such as the color mixing and polarization are derived. Taking the male green peacock (*Pavo* muticus) as an example (Zi et al., 2003), various colors of blue, green, yellow, and brown can be found in the eye pattern of barbules. The coloration in peacock feathers takes the advantage of the partial PBG of the 2D photonic crystal structure in the cortex. Varying the period number leads to the production of additional colors and color mixing. Since natural structural color has been optimized through the millions years evolution, it is efficient to prepare the artificial structure color by learning from the natural coloration strategies and the natural engineering principles.

## NATURE-INSPIRED STRUCTURE-COLOR DESIGN

Natural structural coloration exists in a variety of organisms, including plants, insects, birds, mollusks, sea mice, and fish (Kinoshita, 2008). By regulating the structure morphology, creatures can display the beautiful colors and achieve some specific functions such as camouflage, reproduction, and signal transmission. Along with the growing understanding of the morphology and mechanism of natural structural-color materials, the bioinspired artificial counterparts have been manufactured with improved performance and function consequently (Yang et al., 2017). To our surprise, the various structural colors in nature creatures are made from the limited and ordinary materials such as cellulose, chitin, and keratin (Meyers et al., 2008). The diversity in coloration are basically caused by the well-designed structures (Fudouzi, 2011), which requires highly sophisticated engineering processing at various length scales (Vogel et al., 2015b). In this case, nature can be the teacher of mankind and instruct the artificial structure-color design.

### Iridescent and non-iridescent color design

The phenomenon of iridescence, named the change of color with viewing angles, is a typical property of the natural structural color (Hsiung et al., 2017). Beautiful opals in nature are made from the ordered deposition of spherical silica nanoparticles (NPs) after years of siliceous sedimentation and compression under hydrostatic and gravitational forces (Sanders, 1964). The opal give strong iridescent structural colors by the multiple scattering of light off the periodic planes (Figure 2A), whose wavelength can be defined by the Bragg's law (Richel et al., 2000) as follows

$$M\,\lambda = 2\,d\,(n^2_{\mathrm{eff}} - \sin^2\theta)^{1/2} \qquad \text{(Equation 2)}$$

where $m$ refers to the diffraction order, $\lambda$ is the wavelength of the refracted peak, $d$ is the crystalline interplanar spacing, $n_{\mathrm{eff}}$ is the effective index of refraction, and $\theta$ is the angle between the incident light and a normal line to the opal surface. From the above formula, it is clear that the reflected color is highly dependent of the incident angles.

A great variety of colloidal spheres obtained from the organic and inorganic materials have been exploited to produce the biomimetic opal structures by colloidal crystallization methods (Boles et al., 2016). The vertical or convective deposition is a commonly used strategy (Figure 2B). This technique relies on the capillary forces to organize the colloidal particles during the liquid evaporation, which can induce the assembly of multilayer colloidal PCs. Inverse opal film could be fabricated by the template replication or the coassembly of different materials (Kim et al., 2012). To satisfy the demand for inverse opal film, the size of these filled materials including the ultrafine NPs, precursors of metal oxide, prepolymer solution of hydrogels, and so forth should be much smaller than the channels of the free voids (Zhou and Zhao, 2005). The color of inverse opal film can be purposively tuned by controlling the refractive index contrast on the interparticle medium (Hatton et al., 2010). The coassembly of templating colloidal particles together with a sol–gel matrix precursor material is helpful to release stresses that accumulate during drying and solidification, which enables the formation of highly ordered, large-area, and crack-free films. The crack-free films can present the high-

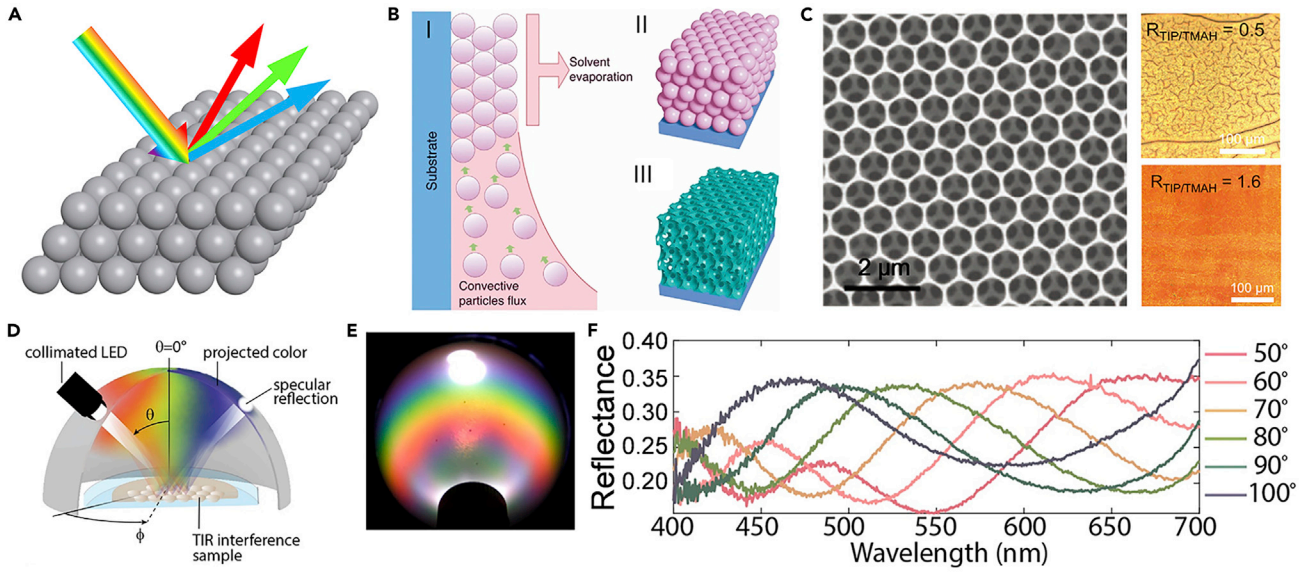


**Figure 2. The iridescent structural color design**

(A) Schematic illustration of the iridescent reflections from the opal structures.

(B) Schematic diagrams of the particle assembly by vertical deposition (I); the assembled opal structure (II); and inverse opal structure after removing the template.

(C) SEM image and the optical photographs of the titania inverse opal films made from nanocrystalline synthesized with different ratios. With the increase of the ratios from 0.5 to 1.6, the high-quality crack-free films can be prepared. Reprinted with permission from Phillips et al. (2018). Copyright 2018, John Wiley & Sons, Inc.

(D–F) Schematic illustration (D) and photograph (E) of the iridescent color distribution in spherical coordinates. Collimated white LED light illuminates the sample through a 3 mm hole in a translucent hemisphere (a half ping-pong ball). The reflected colors are projected onto the inside surface of the translucent hemisphere, which acts as a screen to map the colors; the measured reflection spectra of the sample, showing the angle-resolved feature (F). Reprinted with permission from Goodling et al. (2020). Copyright 2020, American Chemical Society.

quality structure color (Figure 2C). Besides the periodic structures, the individual TIR structure can also display the vivid iridescent color. Goodling et al. fabricated the polymer films composed of microscale dome features that create structural color by interference from TIR. At different viewing and illumination angles, the TIR and interference paths would change, which induced the beautiful iridescent colors (Figures 2D–2F) (Goodling et al., 2020). Similar structures were prepared by partially embedding the polymer microspheres on the sticky side of a transparent tape (Fan et al., 2019). The interferometric effect together with TIR effect that occurred respectively on the embedded and unembedded sections of the microsphere surface resulted in the contrast iridescent colors. Compared with the plant structure colors, the structure colors in animals can present a richer change. Many organisms have developed the unique light manipulation abilities that rely on the sophisticated arrangements of multiscale hierarchical structure (Bae et al., 2014). Taking the butterfly *Pierella luna* as an example, diffraction elements have been found in the wing scales (England et al., 2014). The color appearances of *Morpho* butterflies have also led to advances in several specific applications such as textile, reflectors, cosmetics, and sensing. The wing scales of *Morpho* butterflies are able to exhibit a unique broad blue color, which is the subwavelength scale positional disorder among the multilayered ridges that suppresses the diffraction grating appearance and angle-dependency color (Watanabe et al., 2004).

Although iridescent (or angle-dependent) colors are popular for art and aesthetics, they are not suitable for the development of structural color in displays and sensors, in which stable colors with broad viewing angles are required. Amorphous photonic crystals (APCs) that possess only short-range order show interesting optical responses owing to their unique structural features (Figure 3A) (Shi et al., 2013). The self-assembly of amorphous colloidal arrays has reproduced the non-iridescent structural colors with unique light scattering and transport, which are found in the feathers of some birds or skins of mammals. The caruncles of some birds display non-iridescent blue or green colors, which are arisen from the APCs structures. In the plum-throated *Cotinga*, the back feather barbs contain the three-dimensional APCs consisting of nearly random-close-packed spherical air cavities, which give rise to a vivid non-iridescent turquoise-blue color (Figures 3B and 3C) (Dufresne et al.,

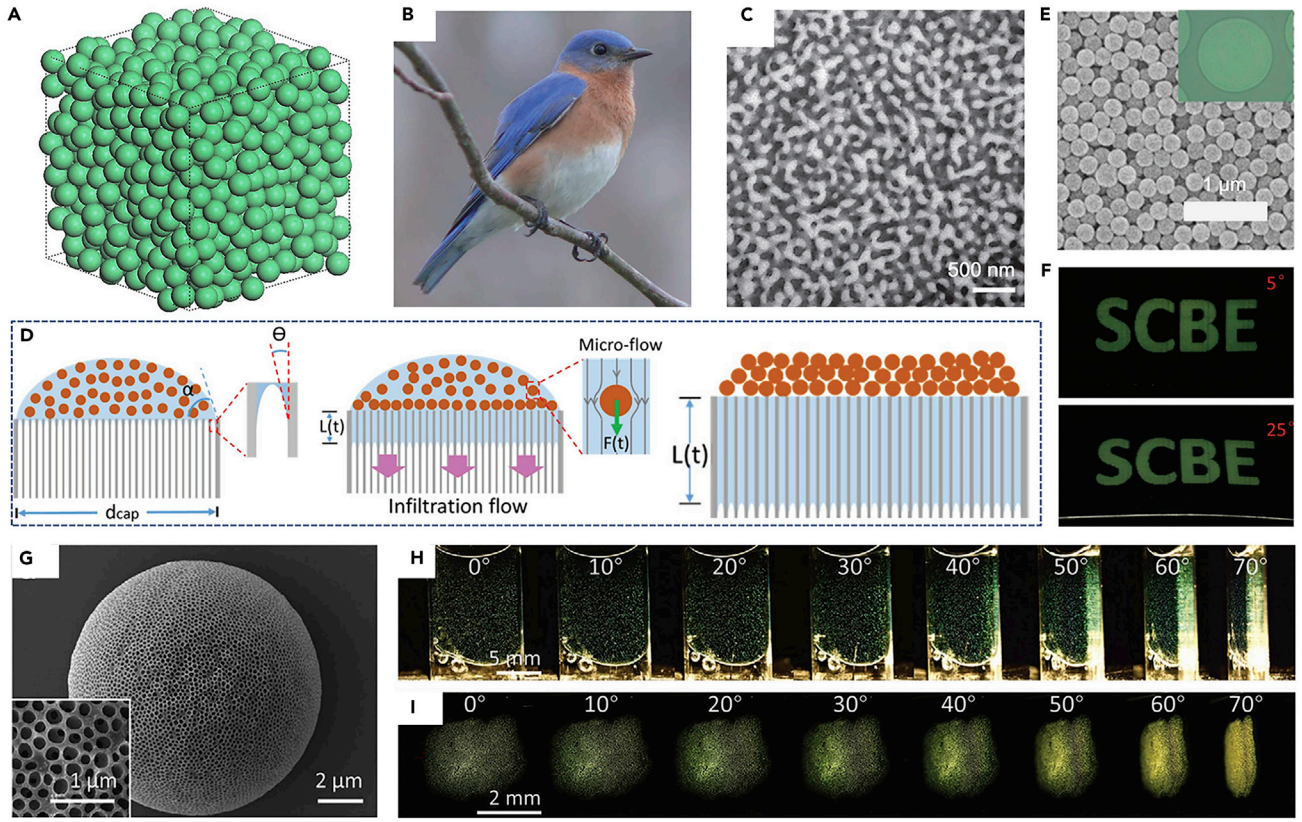


**Figure 3. The bioinspired non-iridescent structural color design**

(A) Schematic illustration of the the amorphous photonic crystals with short-range order.

(B and C) Optical image of Male Eastern Bluebird (Sialia, Turdidae) and SEM image of the channel-type b-keratin and air nanostructure from back contour feather barbs of S. sialis. Reprinted with permission from Dufresne et al. (2009). Copyright 2009, Royal Society of Chemistry.

(D) Illustration of the formation of amorphous colloidal arrays due to a strong downward infiltration flow.

(E) SEM image of a colloidal array prepared on an AAO membrane.

(F) Photographs of inkjet printing SCBE letters at different rotation angles, presenting the angle-independent features. Reprinted with permission from Bai et al. (2018). Copyright 2018, John Wiley & Sons, Inc.

(G) SEM image of the porous surface of the bottlebrush block copolymers microspheres.

(H) An aqueous dispersion of green microspheres inside a flat glass capillary, showing the consistent green color upon rotation of the capillary.

(I) Dried green microspheres on a glass slide, showing the visible green color without any additional refractive index matching. Reprinted with permission from Zhao et al. (2020). Copyright 2020, John Wiley & Sons, Inc.

2009). Inspired by the amorphous solids, there has been considerable interest in constructing the APCs structures with only short-range order to achieve the non-iridescent colors. Duan et al. developed a method for the rapid fabrication of non-iridescent structural colors by non-equilibrium assembly of amorphous colloidal arrays on permeable substrates driven by liquid infiltration (Figure 3D) (Bai et al., 2018). The rapid infiltration of the liquid effectively suppressed the colloidal crystallization and offered vivid non-iridescent colors (Figures 3E and 3F). By introducing a controlled swelling of reverse bottlebrush block copolymer (BBCP) micelles via soft confinement within a toluene in-water microdroplet, Song et al. made the internal aqueous droplets with dimensions comparable to the wavelengths of visible light. Upon subsequent toluene evaporation, the tightly packed nanodroplets could self-assemble to template the formation of a highly porous microparticle (Zhao et al., 2020). The short-range order of the pores within the bottlebrush block copolymers scaffolds (Figure 3G) led to the creation of structural coloration, analogous to inverse photonic glasses. As shown in Figure 3H–3I and 3A consistent green appearance was observed.

## White and black color design

In contrast to brilliant structural color attributed to the selective absorption or reflection of light at specific wavelengths, some species in nature present a broadband reflection and absorption (whiteness and

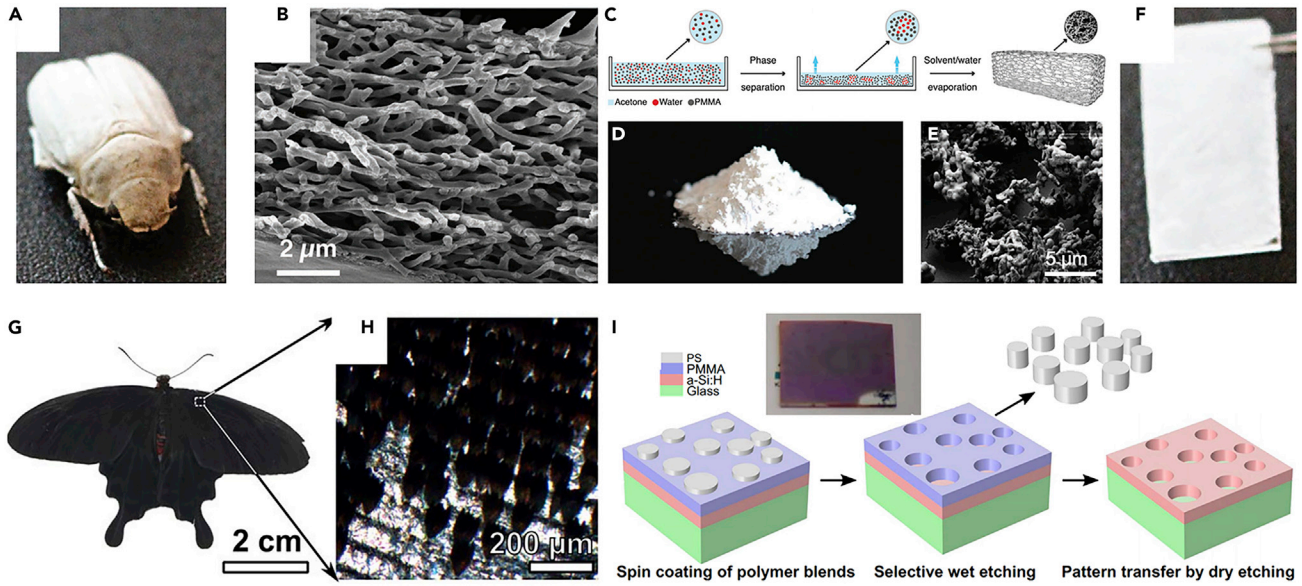


**Figure 4. The bioinspired white and black color design**

(A and B) Photograph of Cyphochilus insulanus beetle and the cross-sectional SEM image of the Cyphochilus scale.

(C) Fabrication route for the bioinspired white films.

(D and E) A photograph of the powder obtained by milling the white PMMA film and SEM image of the powder.

(F) A photograph of the PMMA films (right) exhibiting a bright white appearance. Reprinted with permission from Syurik et al. (2018). Copyright 2018, John Wiley & Sons, Inc.

(G and H) Image of a P.aristolochiae butterfly and the microscopic image of the black region.

(I) Schematic view of the three main fabrication steps including the spin coating of a blend solution of poly(methyl methacrylate) (PMMA) and polystyrene (PS), followed by a selective development of the PS, and finally the transfer of the pattern into a-Si:H by dry etching (RIE). Reprinted with permission from McCoy et al. (2018). Copyright 2018, Springer Nature.

blackness for example) (Morehouse et al., 2007). Random light scattering from disordered structures is responsible for the whiteness of biological species of butterflies and beetles. Many beetles (e.g., *Cyphochilus* and *Lepidiota* stigma) exhibit exceptional bright whiteness, which stems from the randomly arranged and interconnected thin chitin layers. A recent study demonstrated that three impacts were crucial for achieving maximal whiteness with minimal thickness and low refractive index, including the correct network density, the optimal fill fraction, as well as the structural anisotropy (Wilts et al., 2018).

Quids spiders and beetles design the multilayers with varied thickness and spacing to achieve the wavelength-independent broadband reflection. *Cyphochilus* beetles occur widely across Southeast Asia (Figure 4A). The entire exo-skeleton of the beetle is patterned with single wing scales covering the else velvet black exocuticle. These scales strongly scatter the incident light, and the reflectance is basically constant across the visible wavelength range. The scanning electron microscope (SEM) image of the white scales reveals that the scale interior comprises a network of interconnected, chitinous fibers surrounded by air (Figure 4B). Inspired by the natural architectures, Vignolini et al. developed a fast and scalable method to produce the highly scattering porous polymer films via phase separation (Figures 4C–4F) (Syurik et al., 2018). The morphology of the porous films could be modified by varying the polymer molecular weight, and the scattering properties were tuned. They also milled the PMMA porous films into a powder whose particle sizes were below 20 μm. Although the milling process would introduce some change to the film morphology, the powder still kept a rich microstructure (Figure 4E).

Natural examples of structure broadband absorption have been described in the wing scales of butterflies, the body scales of a snake, and the birds of paradise feathers (McCoy et al., 2018). The blackness of butterfly wings was attributed to both the strong absorption of pigmentation and the regulation by micro- and nano-architectures (Figures 4G and 4H). The structurally absorbing materials can generate a super black appearance by increasing the total light absorption or the timing of light scattering. This appearance can be observed from the feathers of several species of birds of paradise. In addition, inspired by the structural

inhomogeneity in the scales of the black butterfly *Pachliopta aristolochiae*, thin photovoltaic absorbers of disordered nanoholes made of hydrogenated amorphous silicon were fabricated by using the method that relied on phase separation of binary polymer mixtures (Figure 4I) (Siddique et al., 2017). The nanopatterned absorbers achieved a relative integrated absorption increase of 90% at a normal incident angle of light, demonstrating the potential for light-harvesting purposes in thin-film solar cells.

## Dynamic color design

Natural structure colors can exhibit the dynamic features. This surprising color allows some organisms to adapt to the needs for living, social interaction, reproduction, and so on (Mason, 2002). One of the most conspicuous species, in terms of the dynamic structure colors, is the chameleon, owning the remarkable ability to exhibit complex and rapid color changes during social interactions such as male contests or courtship (Teyssier et al., 2015). The dynamic color with fast change is resulted from the lattice tuning of guanine nanocrystals within a superficial thick layer of dermal iridophores (Figures 5A–5D). There are two superposed thick layers of iridophore cells in the skin of panther chameleons composed of guanine crystals of different sizes, shapes and organizations. It has been found that the upper layer, which is made of guanine nanocrystals arranged in a triangle lattice, is responsible for the rapid color change. Because the periodic arrangement of guanine and cytoplasm can form the PCs for their different refractive indexes ($n_{guanine}$ = 1.83 and $n_{cytoplasm}$ = 1.33). The color can shift at different states through changing the spacing in the Chameleons lattice. Similarly, Goda et al. has shown that the rapid color change in the chameleon sand tilefish *Hoplolatilus* chlupatyi originates from the change in the spacing between the intracellular reflecting platelets (iridophores) (Goda, 2017).

Inspired by the chameleon, Zhu et al. fabricated a self-healing photonic elastomer with angle-independent structural colors through the combination of a supramolecular elastomer with isotropic nanostructures (Tan et al., 2019). The photonic elastomers could exhibit angle-independent colors, even when Young's modulus and elongation at the break of the as-formed photonic elastomers reached 0.24 MPa and 150%, respectively. This superior elasticity of photonic elastomers enabled their chameleon-skin-like mechanochromic capability with the color gradually changed to green upon stretching and reflection peak gradually shifted from 660 to 550 nm for the lattice change (Figures 5E–5G). Furthermore, during many cycles of stretching and relaxing, the extensional-strain induced color shift was fully reversible and reproducible (Figure 5H), exhibiting its good stability and durability of the photonic elastomers. Yang et al. also prepared a smart window film consisting of a thin layer of quasi-amorphous array of silica NPs embedded in bulk elastomeric polydimethylsiloxane (PDMS) (Ge et al., 2015), which could be reversibly switched from reversibly a highly transparent state (90% transmittance in the visible region) to opaqueness (30% transmittance) (Figures 5I and 5J). The changes in the optical properties were attributed to the microstructure change, including the roughness from wrinkles and nanovoids between PDMS and silica NPs. When stretched, the void around the silica particles formed and the refractive index contrast appeared, inducing an increase of diffused light scattering and absorption. This smart window was promising in many applications such as displays, camouflages, and security, as well as heat/solar gain control.

## Vivid color design

Structure colors have great potentials to replace the toxic conjugated organic dyes and heavy metal pigments due to their anti-fading, smart (e.g., tunable colors with response to stimuli) and eco-friendly advantages. To meet the demand for high-quality structural color products, the gamut, saturation, and brightness of the structure colors need to be improved. Enlightened by the nature's photonic design in avian feathers with vivid colors via the self-assembly of melanosomes, Xiao et al. synthesized and assembled polydopamine-based synthetic melanin NPs into the structure-color films (Figures 6A–6C) (Xiao et al., 2015). The synthetic melanin NPs possessed a high refractive index and broad absorption spanning across the UV visible range, similar to natural melanin. Utilizing a thin-film interference model, the unique optical properties of synthetic melanin NPs were demonstrated, which revealed the color purity and UV-protection advantages over other polymeric NP in constructing structure colors (Figure 6D). Song et al. introduced the graphene nanosheets containing a fraction of graphene quantum dots (GQDs) into the amorphous photonic structures (Zhang et al., 2018) and obtained the highly saturated as well as brilliant non-iridescent structural colors (Figure 6E). The uniform optical absorption of graphene nanosheets contributed to the high saturation of structural color; the wide range tunable photoluminescence (PL) of GQDs manipulated by the pseudo PBG of the APCs realized the wavelength matching and PL enhancement, which improved the peak component intensity (Figures 6F and 6G). When the graphene nanosheets composed of GQDs were doped into the structure-color film, vivid colors on the same white polyvinyl chloride substrate showed (Figure 6H).

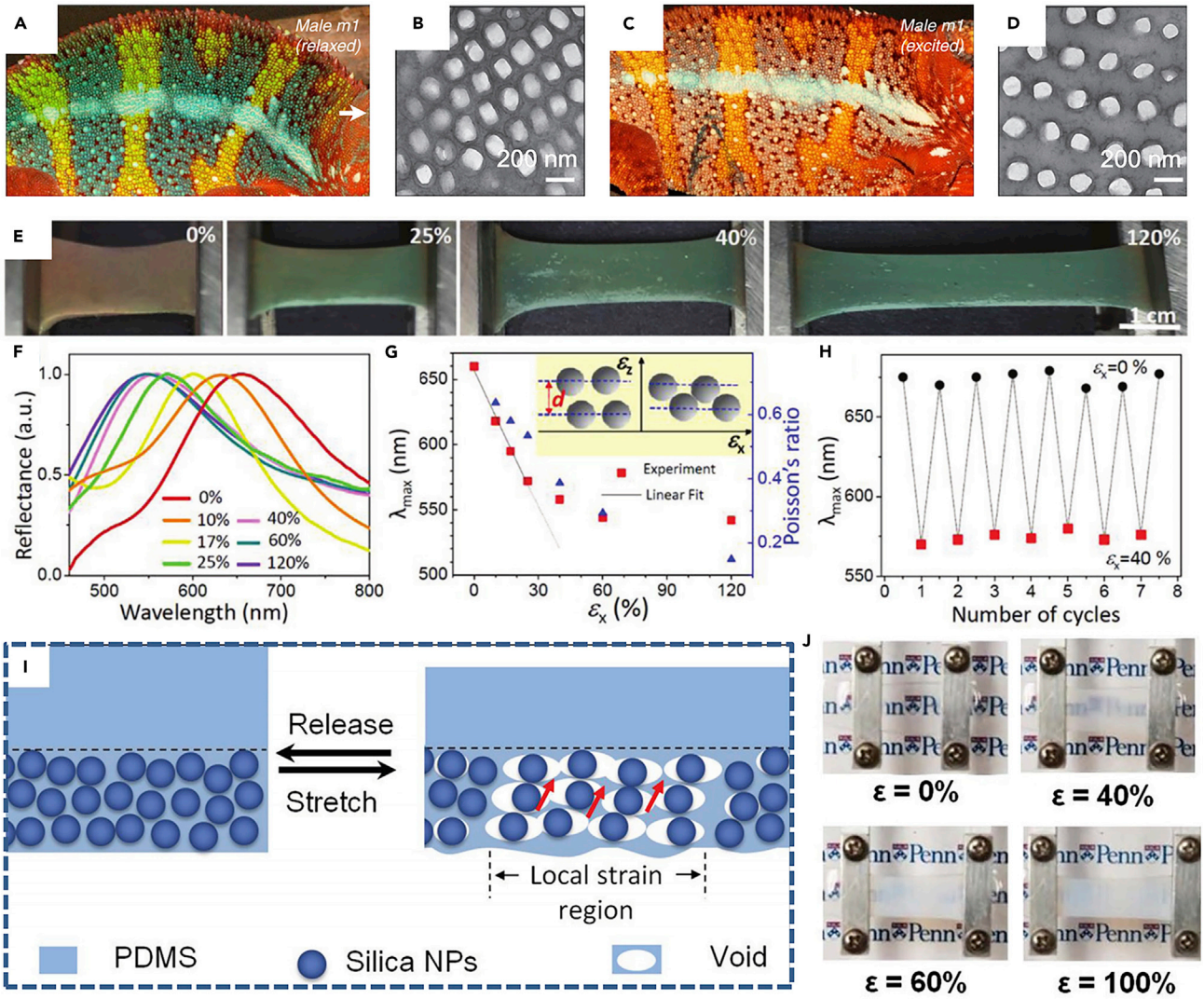


**Figure 5. The bioinspired dynamic color design**

(A–D) Optical photographs (A and C) and TEM images (B and D) of the guanine nanocrystals lattice in the chameleon skin in the relaxed and excited state. Reprinted with permission from Teyssier et al. (2015). Copyright 2015, Springer Nature.

(E and F) Photographs and reflectance spectra of the red color film under various strains (from 0% to 120%).

(G) The peak position of the reflectance spectra ($\lambda_{max}$) and the calculated Poisson's ratio as a function of strain for the red-colored photonic elastomer. Inset shows the strain in x and z direction during a stretching process.

(H) Reversible variation of $\lambda_{max}$ during cycles of extension. Reprinted with permission from Tan et al. (2019). Copyright 2019, John Wiley & Sons, Inc.

(I and J) Schematic illuminates the void formation around the silica particles when stretched and the Photographs of the variation of the composite film at various strains. Reprinted with permission from Ge et al. (2015). Copyright 2015, John Wiley & Sons, Inc.

Fabricating the large-scale PCs with narrow stopbands is highly challenging due to the difficulty in achieving PCs with combined properties of homogeneously well-ordered latex assembly, large-area crack elimination, decreased void fraction, and sufficient thickness (Huang et al., 2012). By using low-adhesive superhydrophobic substrates for the continuous receding of three-phase contact lines of latex suspensions during the evaporation process (Figure 6I), Song et al. fabricated the centimeter scale, well-ordered, and crack-free opals with narrow stopbands (12 nm) (Figure 6J), which induced the vivid PCs structural color (Figure 6K). Moreover, they also constructed the composite architecture combining the 2D PC with a Fabry–Perot cavity and obtained the controllable structure colors with both high saturation and brightness (Figure 6L). The color was derived from the synergistic effect of interference, diffraction, and Rayleigh scattering controlled by the composite structure (Li et al., 2018).

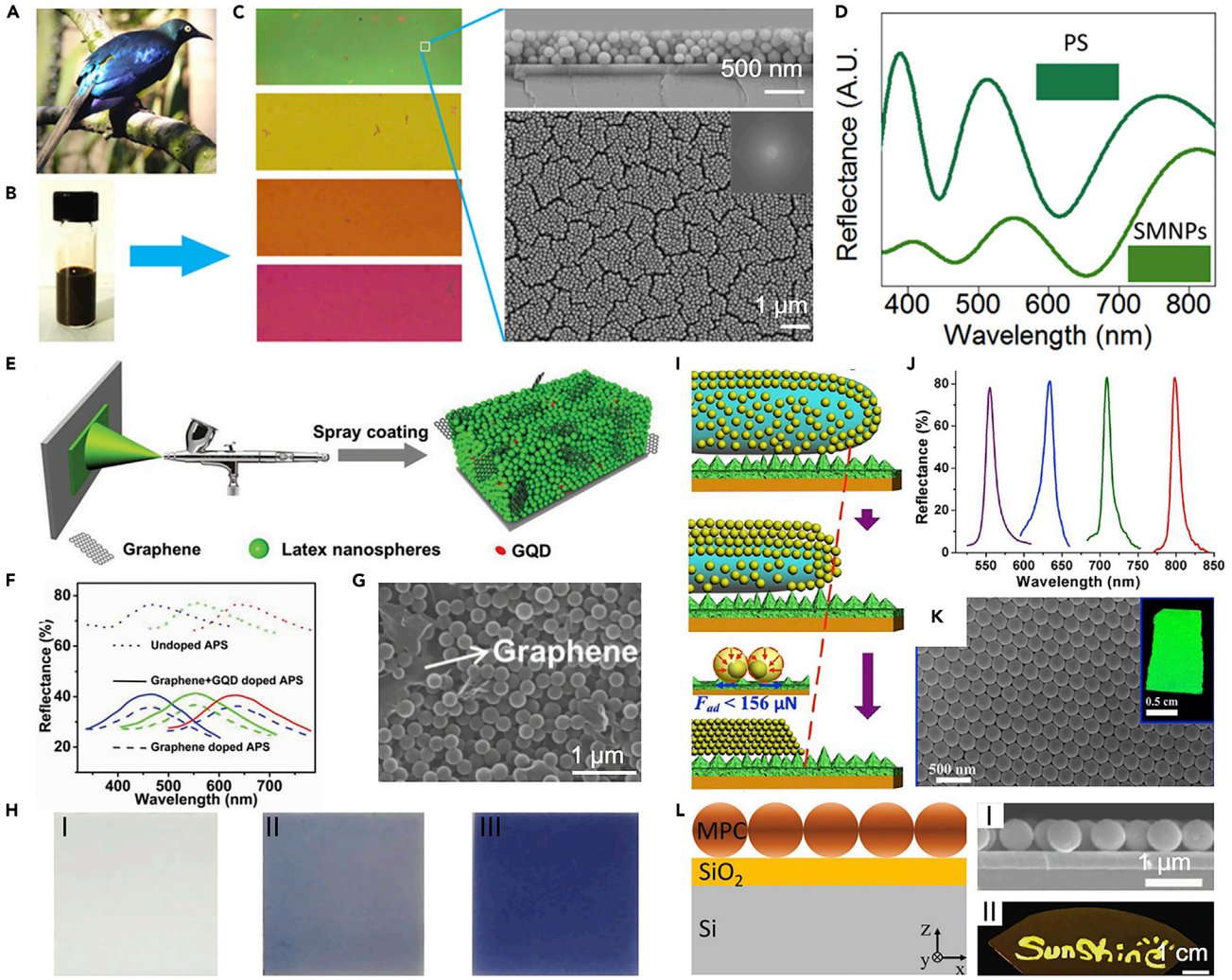


**Figure 6. Vivid color design**

(A and B) Optical photographs of the avian with blue feathers and the melanin nanoparticle ink based on the polydopamine.

(C) Optical images of colored films and SEM images of the frame part in the green film.

(D) Reflectance spectra of polystyrene (PS) nanoparticle film and the synthetic melanin nanoparticles (SMNPs) film. Reprinted with permission from Xiao et al. (2015). Copyright 2015, American Chemical Society.

(E and F) Schematic illustration of the fabrication process by spray-coating and reflectance spectra of the different structural color films without dopant and by graphene nanosheet doping with or without GQDs.

(G and H) SEM image of the as-obtained structural color film and photographs of the undoped films (I) and graphene nanosheet doped structural color films without GQDs (II) and with GQDs (III). Reprinted with permission from Zhang et al. (2018). Copyright 2018, John Wiley & Sons, Inc.

(I) Schematic illustration of colloidal PCs assembled on superhydrophobic substrate with low adhesion.

(J) The reflectance spectra of the assembled high-quality film showing the respective FWHMs of the stopbands of 12, 15, 12, and 12 nm, respectively.

(K) SEM image of perfectly ordered latex arrangement and close-packed assembly structures. Inset is a photograph of a part of the film. Reprinted with permission from Huang et al. (2012). Copyright 2012, American Chemical Society.

(L) Realistic model of the 2DPC-FP composite structure as well as the SEM image of the assembled mono-layer structure and the optical photograph of the golden word "sunshine". Reprinted with permission from Li et al. (2018). Copyright 2018, John Wiley & Sons, Inc.

## CONTROLLABLE FABRICATION OF ARTIFICIAL STRUCTURAL COLORS

Natural structure colors provide us with many wonderful inspirations to design and prepare the artificial structure colors. The colors by the self-assembled colloidal photonic crystals (CPCs) take the advantages of low cost, flexibility, and easy processability, which has shown great potential for new photonic materials and diverse practical applications, such as decorations, displays, storage, optical communication, and even quantum information systems (Li et al., 2019a, 2019b). The artificial CPCs can reflect brilliant colors due to

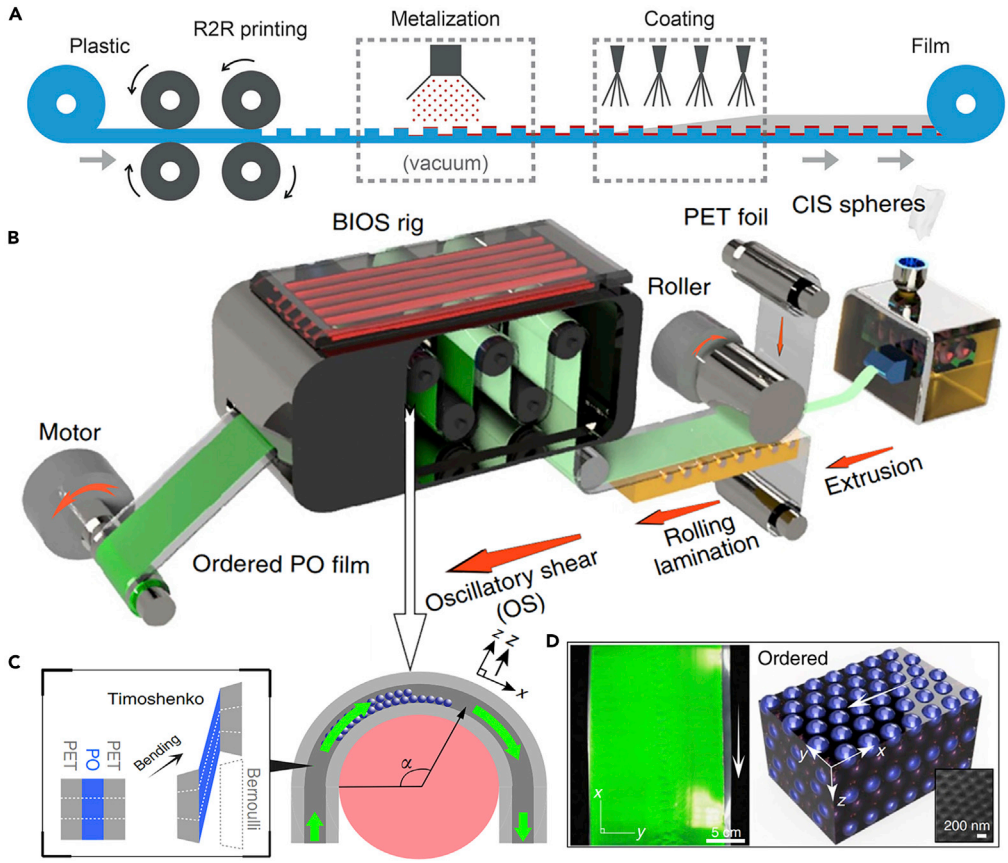


**Figure 7. The large-area preparation of CPCs via roll-to-roll methods**

(A) Schematic illustration of the roll-to-roll printing. Reprinted with permission from Højlund-Nielsen et al. (2016). Copyright 2016, John Wiley & Sons, Inc.

(B) Schematic illustration of the large-scale polymer opals (POs) film with bending-induced oscillatory shear (BIOS) technique.

(C) Mechanism of BIOS inside the PET-PO-PET (PET: polyethylene glycol terephthalate) sandwich, dashed white lines show the bending-induced deformation in different layers.

(D) PO film after the BIOS (left) with improved sphere packing (right), arrow indicates shear direction. Inset SEM image shows the hcp packing at the surface. Reprinted with permission from Zhao et al. (2016). Copyright 2016, Springer Nature.

the PBG, and they are able to be prepared into designable patterns over a large area (Kim et al., 2009). Based on the function demands, we introduce the typical methods to manufacture the CPCs structure colors.

## Roll-to-roll for the large-area manufacturing

As economic color materials, CPCs are promising in practical applications. To realize it, the large-area preparation of CPCs is necessary. So far, many methods for fabricating the CPCs have been developed. In particular, the self-assembly of colloidal particles driven by solution evaporation is widely used (Yu et al., 2012). This method is a bottom-up strategy that can arrange the mono-dispersed particles into close-packed crystals. However, this method usually suffers from the challenge of ubiquitous "coffee ring" phenomenon (Hu and Larson, 2006), which results in the limited pattern resolution and low color saturation. By using the hydrophobic substrate of low surface energy, Marangoni flow, irregular particles, "colloid skin" and so on (Zhang et al., 2019b), this obstacle has been gradually overcome. Nevertheless, the large-area and continuous manufacturing of the CPCs film is still rare. The roll-to-roll techniques have been demonstrated as a suitable method for patterning the large-area coverage, as shown in Figure 7A, which can be used to replicate the high-resolution pattern combined with nanoimprint (Højlund-Nielsen et al., 2016). With the roll-to-roll process, Baumberg et al. developed a bending-induced oscillatory shear (BIOS) technique to achieve the large-area and flexible assembly of stacked polymer NPs (Figure 7B) (Zhao et al., 2016). They prepared

the core-shell spheres by emulsion polymerization and placed the spheres through the standard extrusion-rolling-lamination procedure. To carry out the BIOS process, they constituted a "sandwich" beam composed of the PET-PO-PET laminate (Figure 7C). By bending this laminate around a cylinder, strong shear was created inside the polymer opals purely parallel to the surface. The direction of shear oriented the close-packed lines of spheres in each hexagonal close-packed (*hcp*) plane and controlled the in-plane ordering. After BIOS, the spheres were packed with the most close-packed direction parallel to the x-direction, inducing the brilliant structure colors (Figure 7D). This way opened the door to manufacture the PCs colors continuously and formed a generic tool for ordering the NPs.

## Microfluidics for the controlled preparation of spherical CPCs

Spherical colloidal photonic crystals (SCPCs), due to the spherical symmetry, can conquer the angle-dependent colorations and present the constant PBGs viewing from different angles, broadening their applications in many fields (Zhao et al., 2013). Recently, via the microfluidics, a series of SCPCs materials have been developed including the uniform, Janus, multicomponent, core-shell, inverse opal SCPCs and so on (Wang et al., 2020; Zhao et al., 2014). Microfluidics is a significant strategy for realizing the miniaturization, integration, and intelligentization of chemical and biological sensors (Yeo et al., 2016). It is efficient to prepare the SCPCs by using the droplet templates (Zhang et al., 2019a). As shown in Figure 8A, a capillary microfluidic device is required to generate the microdroplets containing the colloidal particles. Each microdroplet serves as a soft and spherical template to confine the colloidal particles. As the liquid evaporates from the microdroplet, the particles can assemble into close-packed crystals with the spherical morphology (Zhang et al., 2019a). This evaporation-induced colloidal assembly can be regarded as a concentration process, in which the volume fraction of building blocks gradually increases from a low value to a maximum (74%). During the assembly, capillary forces provide a compressive force that leads to the ordered arrangement of the colloidal NPs. Similar to the planer colloidal crystals, the surfaces of the SCPCs also form the (111) plane with the FCC symmetry (Figures 8B and 8C) (Zhao et al., 2006). The size of the SCPCs can be controlled by the initial droplet template size and the NP volume fraction in the initial droplet. Gu et al. have been done a lot of work on preparing the SCPCs. They fabricated various SCPCs by controlling the monodisperse droplets and components, such as the uniform opal and inverse opal SCPCs (Figures 8D–8F) (Zhao et al., 2009). Similar to the inverse opal film, inverse opal SCPCs could be fabricated by template replication or coassembly. Coassembly is implemented by the evaporation of droplets that contain a mixture of the templated polystyrene NPs and a matrix of ultrafine silica NPs. Theoretically, to guarantee that the polystyrene NPs are packed closely to a bead in an fcc arrangement and the ultrafine silica NPs infiltrate all the interstitial sites between the polystyrene NPs, the volume ratio of polystyrene and silica NPs should be about 3.85. However, during the solvent evaporation, the polystyrene NPs escape from the droplet templates more easily than the silica NPs. After solidification, the silica NPs cannot infiltrate all the interstitial sites between the polystyrene NPs. Thus, the ideal practical volume ratio for achieving a successful coassembly is about 9. After removing the polystyrene templates, inverse SCPCs can be formed.

## Printing for the complex patterning

Patterned CPCs contribute to a novel approach for high-performance structural-color devices with unique structures and specific functions. Various strategies to fabricate the patterned CPCs, including etched-substrate induced assembly, printing, selective immobilization and selective modification, are developed (Vogel et al., 2015a). Among them, printing is an additive patterning method, which is able to distribute a broad variety of functional materials onto a desired position directly and efficiently (Gao et al., 2017). Patterning CPCs by printing can be summarized as the drying process of a tiny droplet on a target substrate (Kuang et al., 2014b; Min et al., 2019), where the particle assembly and crystallization will happen. The drying dynamics determines the assembly morphology (Guo et al., 2018) and thus controls the color quality of CPCs patterns.

Kim et al. developed an inkjet printing method that could fabricate the monolayered PCs patterns with extremely weak structural colors (Figures 9A and 9B) (Nam et al., 2016). The mono-layered CPCs patterns were controlled by the ink components (water and formamide), particle concentration and substrate wettability. These factors affected the Marangoni flow in the ink solution and determined the deposited morphology. Through the controlled sliding of the three-phase contact line on a hydrophobic substrate, Song et al. prepared the domed CPCs patterns (Figures 9C and 9D). This domed pattern with angle-independent property is useful for wide viewing angle displays (Kuang et al., 2014a). By patterning hydrophilic

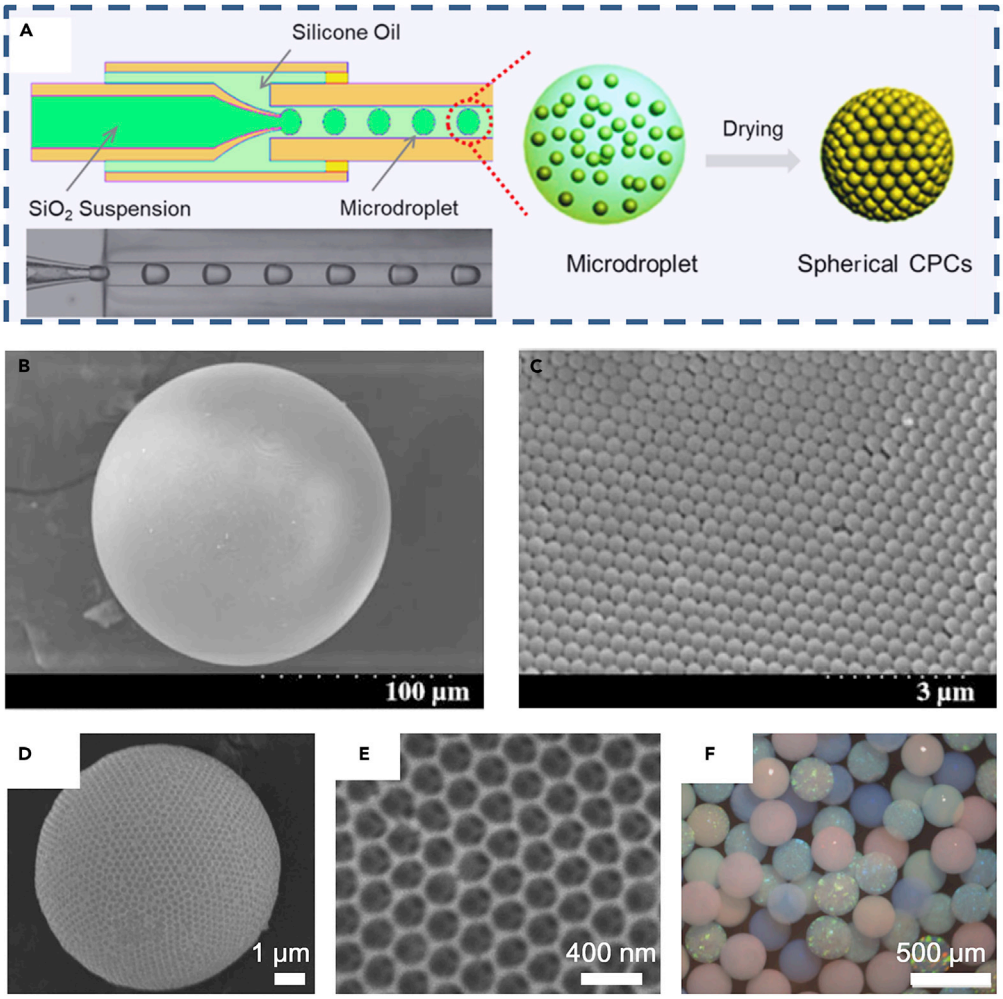


**Figure 8. The preparation of SCPCs via microfluidics assembly**

(A) Schematic illustration of the fabrication of spherical colloidal photonic crystals (SCPCs) by using the droplet-based microfluidic method. Reprinted with permission from Zhang et al. (2019a). Copyright 2019, American Chemical Society.

(B and C) Low-magnification image of the SCPCs showing the smooth bead surface and the high-magnification image of the SCPCs showing the hexagonal alignment of nanoparticles. Reprinted with permission from Zhao et al. (2006). Copyright 2006, John Wiley & Sons, Inc.

(D and E) SEM image of a small inverse opal SCPCs with porous surface and the magnificent SEM image of the inverse SCPCs showing the ordered pore structure inside.

(F) 3D optical image of the seven kinds of inverse opal SCPCs in water. Reprinted with permission from Zhao et al. (2009). Copyright 2009, John Wiley & Sons, Inc.

pinning points on hydrophobic surfaces, they also constructed the controllable 3D micro-CPCs patterns (Wu et al., 2015). By printing MeOH/water on an inverse opal lattice, a patterning silk inverse opal strategy was developed for the generation of multispectral patterns (Li et al., 2019a, 2019b). Via the precise deposition, digitally designed photonic lattice and complex structural-color image were easily achieved (Figures 9E and 9F). By combining the evaporative colloidal assembly with the direct-writing technique, the particle organization with global shape was controlled and the freestanding colloidal structures in centimeter scale were achieved (Figure 9G), enabling the freestanding construction of macroscale CPCs (Figures 9H and 9I) (Tan et al., 2018).

## PROMISING APPLICATIONS OF ARTIFICIAL STRUCTURAL COLORS

After years of research, artificial structural colors have made breakthroughs in various fields for their conspicuous advantages. Bright structural colors have great potential for next-generation display devices.

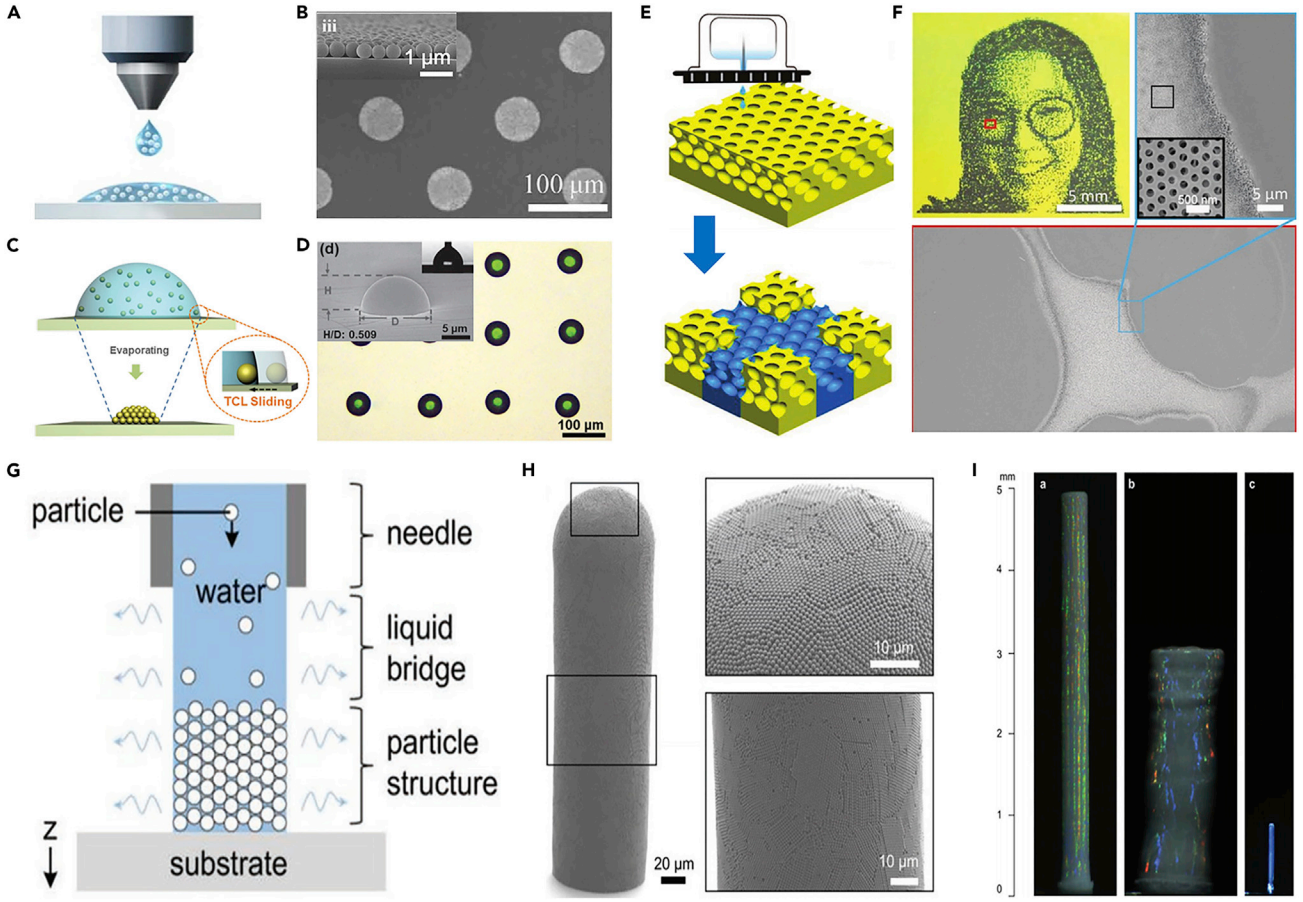


**Figure 9. The patterned CPCs by printing**

(A) Schematic illustration of the preparation of monolayer photonic crystals by inkjet printing.

(B) SEM image of mono-layered photonic crystal array. Inset is the side-view SEM image. Reprinted with permission from Nam et al. (2016). Copyright 2016, Springer Nature.

(C) Schematic illustration of the assembly process of colloidal particles on hydrophobic substrate during solution evaporation.

(D) Optical image of the printed array of domed photonic crystals. Inset is the side-view SEM image. Reprinted with permission from Kuang et al. (2014a). Copyright 2013, John Wiley & Sons, Inc.

(E) Schematic illustration of patterning silk inverse opal by printing the soluble ink.

(F) The optical photograph and SEM image of the printed pattern, showing the portrait morphology and internal structure. Reprinted with permission from Li et al. (2019a, 2019b). Copyright 2019, John Wiley & Sons, Inc.

(G) Schematic illustration of the direct-printing process of the freestanding colloidal crystal structures.

(H) SEM image of a freestanding structure comprising of particles of radius a = 500 nm. Insets: close views of top and middle sections.

(I) Optical images of vertical columns built from colloidal particles with different diameters. Reprinted with permission from Tan et al. (2018). Copyright 2018, John Wiley & Sons, Inc.

Based on an engineered metasurface as a tunable back-reflector, full-color, high-brightness organic lighting emitting diode has been designed with the ultrahigh density of 10,000 pixels per inch (Joo et al., 2020). Due to the fade-resistant nature of structural colors, the structure-color pattern can be used in unique and covert product tagging or decorations. The dynamic features responding to temperature, chemicals, and humidity also make them appropriate visual sensors. In this section, the typical applications of structural-colored materials are introduced, along with a discussion of their functions and advantages.

## Image display

As a promising alternative to pigment or dye ink, the synthetic colloidal particles can be directly used as environmentally friendly paints to make color and decorations (Zhao et al., 2019). By controlling the chemical synthesis process, the colloidal particles with adjustable diameters can be obtained from various materials,

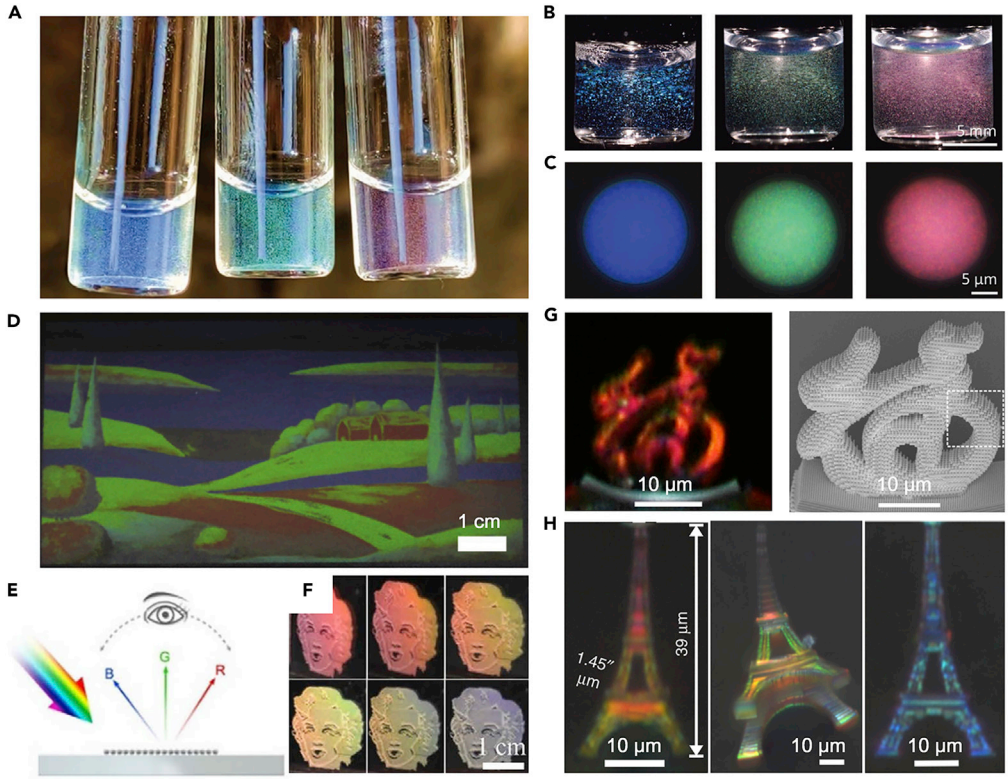


**Figure 10. The image display based on the artificial structural colors**

(A and B) The blue, green and red structure-color inks illuminated by natural sunlight and epi-illumination.

(C) Microscopy images of individual microspheres collected in epi-illumination. Reprinted with permission from Zhao et al. (2020). Copyright 2020, John Wiley & Sons, Inc.

(D) The printed multicolored painting of a landscape with high resolution. Reprinted with permission from Bai et al. (2018). Copyright 2018, John Wiley & Sons, Inc.

(E and F) Schematic illustration and optical images of the printed iridescent pattern by manipulating the illumination and background conditions. Reprinted with permission from Nam et al. (2016). Copyright 2016, Springer Nature.

(G) Optical micrograph and SEM image of a 3D Chinese character "福" with red color.

(H) Micrographs of printed 3D model of the Eiffel Tower with different colors. Reprinted with permission from Liu et al. (2019). Copyright 2019, Springer Nature.

such as polystyrene, polymethyl methacrylate, silica, zinc oxide, and so on (Ciriminna et al., 2013). Owing to the capability of chemical synthesis and the wide range of material sources, the colloidal particles are designed and fabricated with specific functions, such as improving the color saturation, the UV resistance, the responding speed and mechanical behaviors. The colloidal particle emulsion can be directly printed on the target substrate to prepare the exquisite painting and specific trademarks (Figures 10A–10C). By controlling the assembly morphology, the color of the printed image can be non-iridescent (Figure 10D) or iridescent (Figures 10E and 10F). For the advantages of various colors at different viewing conditions, the printed images designed by inkjet printers would not only produce optical holograms for the simple authentication of many items and products but also enable a high-secure anti-counterfeit technique. By introducing a heat-shrinking method, 3D-printed PCs with sub-100-nm features were achieved across a full range of colors (Liu et al., 2019). With these lattice structures as color volumetric elements, 3D microscopic scale objects, including a 20 μm tall Chinese character for luck "福" (Figure 10G) and a multi-color microscopic model of the Eiffel Tower measuring only 39 μm tall with a color pixel size of 1.45 μm (Figure 10H) were fabricated. The 3D PCs could exhibit rich color variations in three-dimensional space.

## Information security

Information security is a perpetual concern for both individuals and the public. Coding is an efficient strategy to protect the information from leakage and falsification and is widely used in secure communication

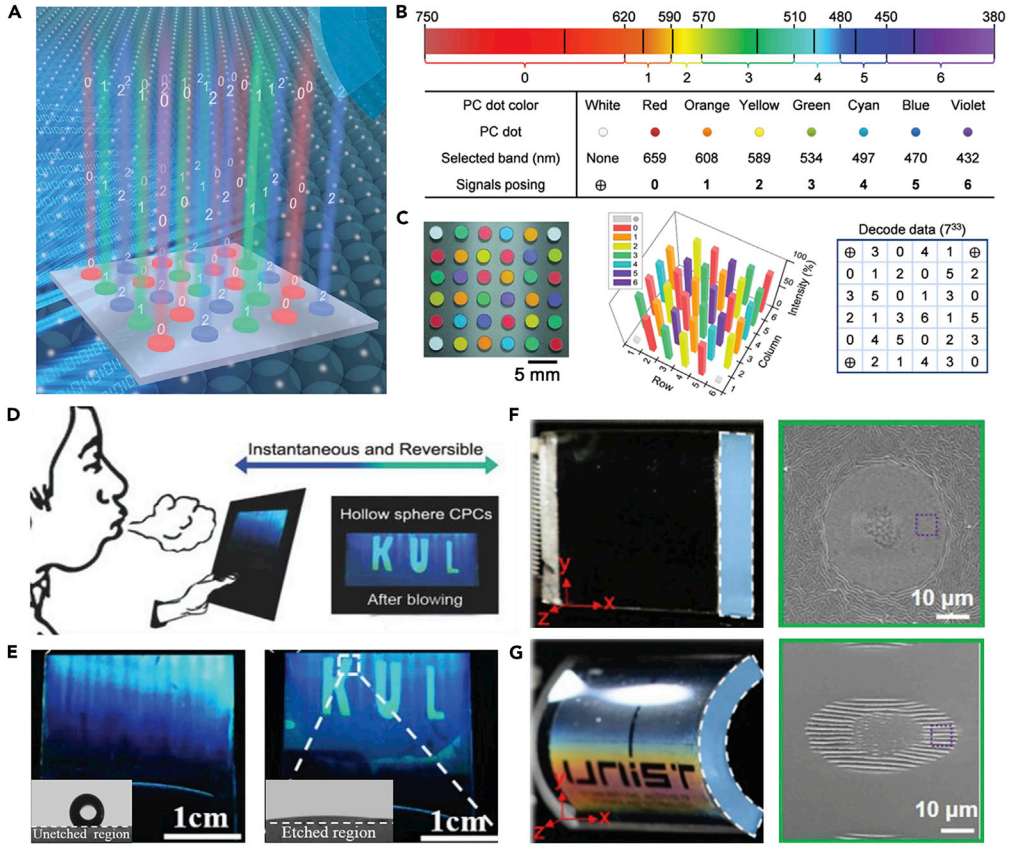


**Figure 11. Information security with the artificial structural colors**

(A) Illustration of the relationship between the displayed color with the information code.

(B) The pre-built congruent relationship between the optical stopband and digital signal.

(C) Septenary PC coding system formed by encoding the PC dots with more distinguishable stopbands. Reprinted with permission from Li et al. (2017). Copyright 2017, Royal Society of Chemistry.

(D) Illustration of the presentation of the hidden information after blowing.

(E) Optical images of the prepared sample before and after a breath. Insets are the microscopic images of the droplet (2 μL) deposited on the sample surface of unetched (Left) and etched (Right) regions, showing the contrast wettability. Reprinted with permission from Zhong et al. (2018). Copyright 2018, John Wiley & Sons, Inc.

(F) Optical and SEM images of the transparent SiO2-NP/PDMS composite device in the normal state.

(G) Optical and SEM images of the same device with colorful information when the patterned side is bent. Reprinted with permission from Zhou et al. (2020). Copyright 2020, John Wiley & Sons, Inc.

and anti-counterfeiting. Unlike the chemical color materials such as fluorescent molecules or quantum dots, the photonic stopband-based structural colors have an outstanding stability without the photobleaching and agglomeration (Wang et al., 2006). This optical property is very important for information security, especially for improving the coding capacity and security level (Qi et al., 2019).

By building the coding relationship between the photonic stopbands and information units, the messages can be hidden in the PCs patterns (Li et al., 2017).

The basic principle for designing the PC coding system relies on the corresponding coding connection (Figures 11A). By marking the stopband with a binary or multi-level numerical system, the designed PCs dot pattern with different stopbands was used for information recording (Figures 11B). According to the predetermined relationship, the PCs coding pattern that consists of seven different stopbands could be translated into digital information (Figures 11C). Besides the visible information coding, the PCs color can also be applied to the information encryption and hiding due to the dynamic property (Zhong et al., 2018). The information hiding could be implemented by constructing the hydrophilic pattern on a PC-based hydrophobic substrate (Figures 11E). The message was totally invisible for the same morphology

between the patterned region and the blank area. After the easy human breath, the refractive index of the hydrophilic region would change for the sensitivity to humid and the "KUL" letters were immediately revealed in a green color (Figures 11D).

Furthermore, Kim et al. exploited the external mechanical stimuli to control the stealth and display of structure-color pattern and achieved a flexible switching between transparent and colored states (Zhou et al., 2020). They fabricated a composite laminate composed of soft PDMS and a printed information pattern of rigid SiO2-NP assembled structure as the multidimensional structural color platform. This composite film was fully transparent in the normal state due to the similar optical refractive index of PDMS and SiO2 NPs (Figures 11F). However, upon compressive loading, a buckling-type instability appeared on the surface of the laminate, leading to the generation of 1D or 2D wrinkled patterns in the form of gratings and thus the display of hidden pattern (Figures 11G), which was a simple, convenient, inexpensive, and mass-producible manner for anti-counterfeiting applications.

## Real-time visual monitoring

The real-time monitoring is very important for security, traffic, medicine, and so on. The dynamic structure colors responding to environment changes can transform the different external stimuli such as mechanics, temperature, chemical, and humidity to visual color change (Ge and Yin, 2011). Taking the mechanical responsive structural colors as an example, invisible mechanical stimuli such as stretching, compression, or bending in the materials are able to be visualized due to the deformation-induced changes in periodic lattice contained in the structural-colored materials. In particular, the stopband of PC-based structure color can be reversibly changed in response to electricity, magnetism, temperature, pH, ionic species, mechanical effects, glucose, solvents, and so on, which have attracted wide research interest in fundamental researches and potential applications (Wang and Zhang, 2013). Ge et al. developed an electric-filed-assisted multicolor printing based on the electrically responsive and photocurable colloidal PC, which is prepared by the self-assembly of $SiO_2$ particles in the mixture of propylene carbonate and trimethylolpropane ethoxylate triacrylate (Chen et al., 2017). By changing the voltage of the applied electric field, the dynamic equilibrium between the electrical packing force and electrostatic repulsive force were tunned, which resulted in a certain interparticle distance and thus a specific structural color (Figure 12A). With this method, multicolor and high-resolution photonic patterns using a single component could be achieved and was promising to prepare fine patterns in a rapid and low-cost way (Figures 12B and 12C). Similar regulation of structure color was achieved with the magnetochromatic microspheres through instant assembly of superparamagnetic colloidal particles inside emulsion droplets of UV curable resin. Yin et al. prepared the $Fe_3O_4$@$SiO_2$ core/shell particles and assembled them into one-dimensional chains, each of which contains periodically arranged particles diffracting visible light and displaying field-tunable colors (Ge et al., 2009). Because the superparamagnetic chains tend to align themselves along the field direction, the orientation of such photonic microspheres could be easily controlled. Thus, their diffractive colors, by changing the orientation of the crystal lattice relative to the incident light, were regulated by using the magnetic fields. The diffraction of the microspheres dispersed in a liquid can be conveniently switched between "on" and "off" states by using the external magnetic field, as shown in the schematic illustrations and optical microscopy images in Figure 1D. Song et al. prepared a visual humidity sensor based on hydrogel (Tian et al., 2008). For the sensitive property of hydrogel to humidity, the color of the humidity sensor could be reversibly varied from transparent to violet, blue, cyan, green and red under the humidity conditions of 20%, 50%, 70%, 80%, 90% and 100%, respectively, covering the whole visible range. When it dried fully at a humidity of 20%, the film returned to transparent with good durability during tens of cyclic experiments (Figures 12E–12G). Besides the external triggers, Zhao et al. developed the colorful soft robotics by using the biohybrid structural color hydrogel (Fu et al., 2018). They fabricated a self-actuated, 3D artificial *Morpho* butterfly composed of inverse opal-structured hydrogel and cardiomyocytes. The cardiomyocytes formed an anisotropic laminar organization in the direction of the microgrooves and provided corresponding anisotropic and synchronous contractions, as well as relaxations to the substrate. With the bending of the wings, a gradual blue-shift of the reflection peak from the inside to the outer edge could be observed. Also, during one myocardial cycle, the different bending angles corresponded to specific reflection wavelengths for a certain fixed position, which served as unique structural color fingerprints. Moreover, Wu et al. applied the structural color material to a smart, energy-efficient, and tunable nighttime traffic sign based on the iridescent property of structure color (Fan et al., 2019). At night, the smart traffic signs could deliver distance signals coded by color to drivers and pedestrians in real time.

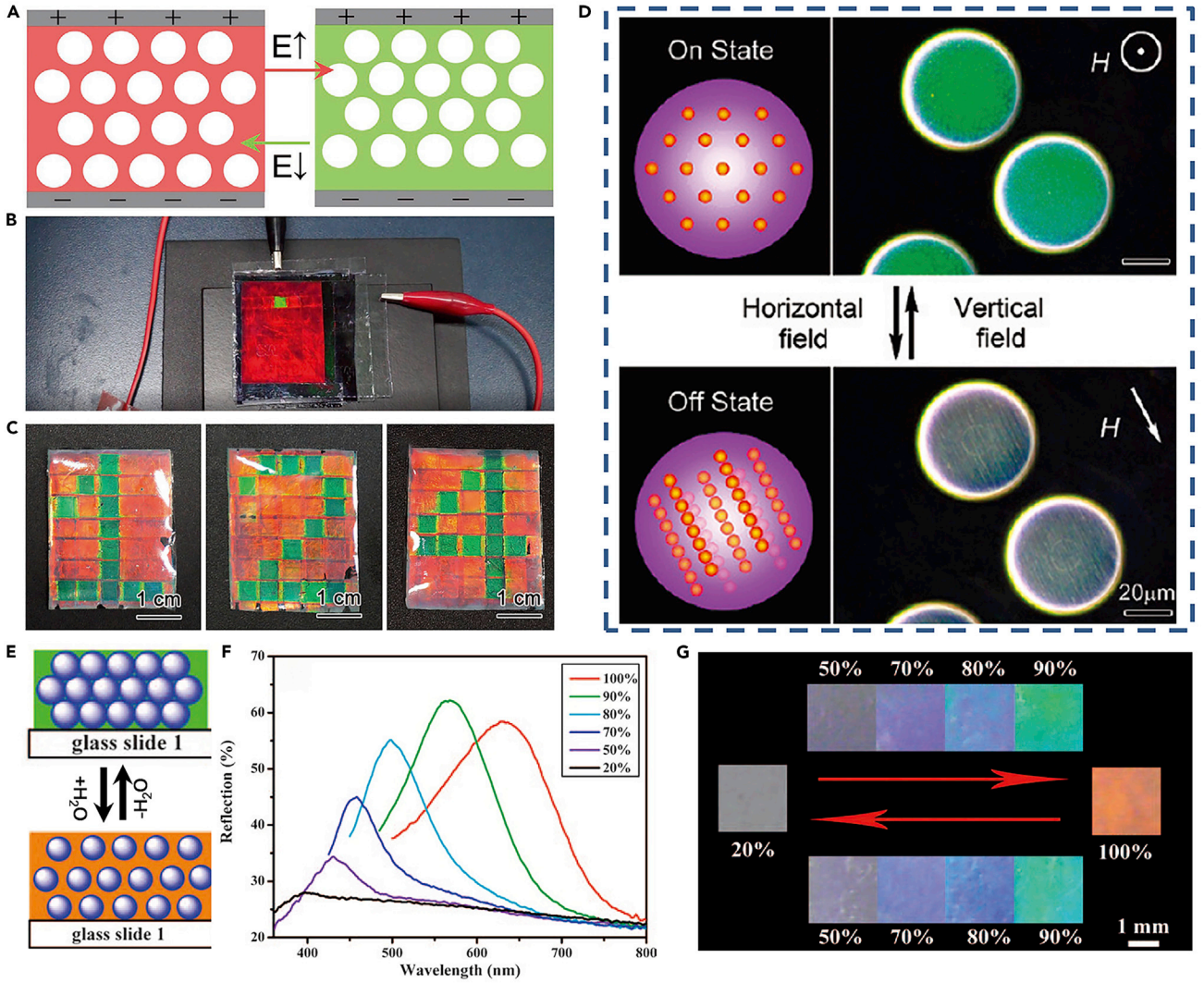


**Figure 12. Real-time visual monitoring with the artificial structural colors**

(A) Schematic illustration to the shrinkage or expansion of colloidal microcrystals as the electric field is increased or decreased.

(B and C) Practical device for the pixel printing of number 1, 2, and 4 in a 5 × 7 array of electric cells. Reprinted with permission from Chen et al. (2017). Copyright 2017, John Wiley & Sons, Inc.

(D) Schematic illustrations and optical microscopy images for the magnetochromatic effect caused by rotating the chain-like photonic structures in magnetic fields. Reprinted with permission from Ge et al. (2009). Copyright 2009, American Chemical Society.

(E) Schematic illustration of the periodic structure change of photonic crystal hydrogel before and after fully wetted in water.

(F) UV-vis spectra of the films under various humidity conditions.

(G) Photographs of the as-prepared PC hydrogel corresponding to relative humidities of 20%, 50%, 70%, 80%, 90% and 100%, respectively. Reprinted with permission from Tian et al. (2008). Copyright 2008, Royal Society of Chemistry.

## CONCLUSION AND OUTLOOK

In this review, we summarize the recent advances in bioinspired structure colors, including the mechanism, the structure design, the fabrication processing, and the application. Since great efforts have been made in this area, various artificial structure colors with fantastic properties are achieved, including the angle-dependent and the angle-independent colors, the ultra-white and the ultra-black colors, the highly saturated or the highly illuminant structure colors. By introducing the smart materials to the photonic systems, responsive structure colors are realized. They can change the displayed color with a certain external stimulus, for instance, the light, the humidity, the temperature, the electrical field, the magnetic field, and so on. These structure-color advancements show the great potential in practical application. And for the structure-color commercialization, great efforts should be made to develop a facile and low-cost method to

manipulate the structure color, such as the roll-to-roll way to continuously manufacture the large-scale structure color, the microfluidics strategy to specifically make the spherical photonic crystal color for some non-iridescent demands, and printing method to construct the structure-color patterns. Based on those technologies, plenty of artificial structure colors come out and realize the applications in imaging, anti-counterfeiting, camouflage, sensing, as well as real-time monitoring.

Even though remarkable advances have been achieved in recent years, further exploration is still highly required in some fields. First, it remains a big challenge to prepare the artificial structure color with high saturation and high brightness simultaneously since there is a trade-off between these two sides. Second, for responsive color systems, most of the smart materials are based on polymers limited to the low refractive indexes. As a result, it is difficult to fabricate a strong reflectance colors with a high contrast, not to mention the absolute PBG (Hu et al., 2020). Although the colloidal diamond has been assembled by using the tetrahedrally coordinated particles, the gap from the research to the commercialization remains extremely large, requiring a more general method (He et al., 2020). Some inorganic responsive NPs have high refractive index, like the magnetic-responsive $Fe_3O_4$ NPs. However, the color based on the $Fe_3O_4$ NPs is difficult to regulate due to the intrinsic property of the particle (Wang et al., 2015). Third, the responsive materials including the hydrogel, electro-responsive elastomers, require a long response and recovery time, which limits these responsive materials in timely monitoring, display, etc. Fourth, even though many groups have been able to make beautiful color patterns, the accurate replication of structure-color image with high fidelity is extremely difficult because fabricating and adjusting the structure-color pixels are very complicated. We need to explore new facile and low-cost color technologies to achieve the complex structural-color pattern. In the end, the devices based on the chromatic material need to be further integrated with other technologies, such as the AI, optic analytical instruments, to realize the immediate readouts of optical signals and sophisticated analysis. If these challenges are overcome, it is believed that the artificial structure color will provide great convenience for our life and contribute a lot to the society.

## ACKNOWLEDGMENTS

The authors would like to thank the National Natural Science Foundation of China (Grant No. 22073107, 51573192, 51773206, 91963212, and 51961145102), National Key R&D Program of China (Grant No. 2018YFA0208501, 2016YFB0401603), Beijing Natural Science Foundation (Grant No.2194093), the China Postdoctoral Science Foundation (2018M641482), K. C. Wong Education Foundation, and Beijing National Laboratory for Molecular Sciences (No. BNLMS-CXXM-202005).

## AUTHOR CONTRIBUTIONS

All authors (K.X.L., C.L., H.Z.L., M.Z.L., and Y.L.S.) jointly discussed the paper and contributed to the original and revised drafts.

## DECLARATION OF INTERESTS

The authors declare no competing interests.

## REFERENCES

Aguirre, C.I., Reguera, E., and Stein, A. (2010). Tunable colors in opals and inverse opal photonic crystals. Adv. Funct. Mater. *20*, 2565–2578.

Bae, W.G., Kim, H.N., Kim, D., Park, S.H., Jeong, H.E., and Suh, K.Y. (2014). 25th anniversary article: scalable multiscale patterned structures inspired by nature: the role of hierarchy. Adv. Mater. *26*, 675–700.

Bai, L., Mai, V.C., Lim, Y., Hou, S., Möhwald, H., and Duan, H. (2018). Large-scale noniridescent structural color printing enabled by infiltration-driven nonequilibrium colloidal assembly. Adv. Mater. *30*, 1705667.

Boles, M.A., Engel, M., and Talapin, D.V. (2016). Self-assembly of colloidal nanocrystals: from intricate structures to functional materials. Chem. Rev. *116*, 11220–11289.

Botten, I., Craig, M., McPhedran, R., Adams, J., and Andrewartha, J. (1981). The dielectric lamellar diffraction grating. Optica Acta Int. J. Opt. *28*, 413–428.

Chen, K., Fu, Q., Ye, S., and Ge, J. (2017). Multicolor printing using electric-field-responsive and photocurable photonic crystals. Adv. Funct. Mater. *27*, 1702825.

Chen, C., Airoldi, C.A., Lugo, C.A., Bay, R.K., Glover, B.J., and Crosby, A.J. (2020). Flower inspiration: broad-angle structural color through tunable hierarchical wrinkles in thin film multilayers. Adv. Funct. Mater. 2006256.

Ciriminna, R., Fidalgo, A., Pandarus, V., Beland, F., Ilharco, L.M., and Pagliaro, M. (2013). The sol–gel route to advanced silica-based materials and recent applications. Chem. Rev. *113*, 6592–6620.

Daqiqeh Rezaei, S., Dong, Z., You En Chan, J., Trisno, J., Ng, R.J.H., Ruan, Q., Qiu, C.-W., Mortensen, N.A., and Yang, J.K. (2020). Nanophotonic Structural Colors (ACS Photonics).

Dufresne, E.R., Noh, H., Saranathan, V., Mochrie, S.G., Cao, H., and Prum, R.O. (2009). Self-assembly of amorphous biophotonic nanostructures by phase separation. Soft Matter *5*, 1792–1795.

England, G., Kolle, M., Kim, P., Khan, M., Muñoz, P., Mazur, E., and Aizenberg, J. (2014). Bioinspired micrograting arrays mimicking the

reverse color diffraction elements evolved by the butterfly Pierella luna. Proc. Natl. Acad. Sci. U S A *111*, 15630–15634.

Fan, W., Zeng, J., Gan, Q., Ji, D., Song, H., Liu, W., Shi, L., and Wu, L. (2019). Iridescence-controlled and flexibly tunable retroreflective structural color film for smart displays. Sci. Adv. *5*, eaaw8755.

Fenzl, C., Hirsch, T., and Wolfbeis, O.S. (2014). Photonic crystals for chemical sensing and biosensing. Angew. Chem. Int. Edit. *53*, 3318–3335.

Foresi, J., Villeneuve, P.R., Ferrera, J., Thoen, E., Steinmeyer, G., Fan, S., Joannopoulos, J., Kimerling, L., Smith, H.I., and Ippen, E. (1997). Photonic-bandgap microcavities in optical waveguides. Nature *390*, 143–145.

Fu, F., Shang, L., Chen, Z., Yu, Y., and Zhao, Y. (2018). Bioinspired living structural color hydrogels. Sci. Robot. *3*, eaar8580.

Fudouzi, H. (2011). Tunable structural color in organisms and photonic materials for design of bioinspired materials. Sci. Technol. Adv. Mater. *12*, 064704.

Gao, M., Li, L., and Song, Y. (2017). Inkjet printing wearable electronic devices. J. Mater. Chem. C *5*, 2971–2993.

Ge, J., and Yin, Y. (2011). Responsive photonic crystals. Angew. Chem. Int. Edit. *50*, 1492–1522.

Ge, J., Hu, Y., and Yin, Y. (2007). Highly tunable superparamagnetic colloidal photonic crystals. Angew. Chem. *119*, 7572–7575.

Ge, J., Lee, H., He, L., Kim, J., Lu, Z., Kim, H., Goebl, J., Kwon, S., and Yin, Y. (2009). Magnetochromatic microspheres: rotating photonic crystals. J. Am. Chem. Soc. *131*, 15687–15694.

Ge, D., Lee, E., Yang, L., Cho, Y., Li, M., Gianola, D.S., and Yang, S. (2015). A robust smart window: reversibly switching from high transparency to angle-independent structural color display. Adv. Mater. *27*, 2489–2495.

Goda, M. (2017). Rapid integumental color changes due to novel iridophores in the chameleon sand tilefish Hoplolatilus chlupatyi. Pigment Cell Melanoma Res. *30*, 368–371.

Goerlitzer, E.S., Klupp Taylor, R.N., and Vogel, N. (2018). Bioinspired photonic pigments from colloidal self-assembly. Adv. Mater. *30*, 1706654.

Goodling, A.E., Nagelberg, S., Kaehr, B., Meredith, C.H., Cheon, S.I., Saunders, A.P., Kolle, M., and Zarzar, L.D. (2019). Colouration by total internal reflection and interference at microscale concave interfaces. Nature *566*, 523–527.

Goodling, A.E., Nagelberg, S., Kolle, M., and Zarzar, L.D. (2020). Tunable and responsive structural color from polymeric microstructured surfaces enabled by interference of totally internally reflected light. ACS Macro Lett. *2*, 754–763.

Guo, D., Zheng, X., Wang, X., Li, H., Li, K., Li, Z., and Song, Y. (2018). formation of multicomponent size-sorted assembly patterns by tunable templated dewetting. Angew. Chem. *130*, 16358–16362.

Hatton, B., Mishchenko, L., Davis, S., Sandhage, K.H., and Aizenberg, J. (2010). Assembly of large-area, highly ordered, crack-free inverse opal films. Proc. Natl. Acad. Sci. U S A *107*, 10354–10359.

He, M., Gales, J.P., Ducrot, É., Gong, Z., Yi, G.-R., Sacanna, S., and Pine, D.J. (2020). Colloidal diamond. Nature *585*, 524–529.

Højlund-Nielsen, E., Clausen, J., Mäkela, T., Thamdrup, L.H., Zalkovskij, M., Nielsen, T., Li Pira, N., Ahopelto, J., Mortensen, N.A., and Kristensen, A. (2016). Plasmonic colors: toward mass production of metasurfaces. Adv. Mater. Technol. *1*, 1600054.

Hong, W., Yuan, Z., and Chen, X. (2020). Structural color materials for optical anticounterfeiting. Small *16*, 1907626.

Hou, J., Li, M., and Song, Y. (2018). Patterned colloidal photonic crystals. Angew. Chem. Int. Edit. *57*, 2544–2553.

Hsiung, B.-K., Siddique, R.H., Stavenga, D.G., Otto, J.C., Allen, M.C., Liu, Y., Lu, Y.-F., Deheyn, D.D., Shawkey, M.D., and Blackledge, T.A. (2017). Rainbow peacock spiders inspire miniature super-iridescent optics. Nat. Commun. *8*, 1–8.

Hu, H., and Larson, R.G. (2006). Marangoni effect reverses coffee-ring depositions. J. Phys. Chem. B *110*, 7090–7094.

Hu, F., Lin, N., and Liu, X. (2020). Interplay between light and functionalized silk fibroin and applications. Iscience, 101035.

Huang, Y., Zhou, J., Su, B., Shi, L., Wang, J., Chen, S., Wang, L., Zi, J., Song, Y., and Jiang, L. (2012). Colloidal photonic crystals with narrow stopbands assembled from low-adhesive superhydrophobic substrates. J. Am. Chem. Soc. *134*, 17053–17058.

Isapour, G., and Lattuada, M. (2018). Bioinspired stimuli-responsive color-changing systems. Adv. Mater. *30*, 1707069.

Ji, C., Lee, K.T., Xu, T., Zhou, J., Park, H.J., and Guo, L.J. (2017). Engineering light at the nanoscale: structural color filters and broadband perfect absorbers. Adv. Opt. Mater. *5*, 1700368.

Joannopoulos, J.D., Villeneuve, P.R., and Fan, S. (1997). Photonic crystals: putting a new twist on light. Nature *386*, 143–149.

Joo, W.-J., Kyoung, J., Esfandyarpour, M., Lee, S.-H., Koo, H., Song, S., Kwon, Y.-N., Song, S.H., Bae, J.C., and Jo, A. (2020). Metasurface-driven OLED displays beyond 10,000 pixels per inch. Science *370*, 459–463.

Kim, H., Ge, J., Kim, J., Choi, S.-e., Lee, H., Lee, H., Park, W., Yin, Y., and Kwon, S. (2009). Structural colour printing using a magnetically tunable and lithographically fixable photonic crystal. Nat. Photon. *3*, 534–540.

Kim, S., Mitropoulos, A.N., Spitzberg, J.D., Tao, H., Kaplan, D.L., and Omenetto, F.G. (2012). Silk inverse opals. Nat. Photon. *6*, 818–823.

Kinoshita, S. (2008). Structural Colors in the Realm of Nature (World Scientific).

Kinoshita, S., and Yoshioka, S. (2005). Structural colors in nature: the role of regularity and irregularity in the structure. ChemPhysChem *6*, 1442–1459.

Kinoshita, S., Yoshioka, S., and Miyazaki, J. (2008). Physics of structural colors. Rep. Prog. Phys. *71*, 076401.

Kolle, M., Salgard-Cunha, P.M., Scherer, M.R., Huang, F., Vukusic, P., Mahajan, S., Baumberg, J.J., and Steiner, U. (2010). Mimicking the colourful wing scale structure of the Papilio blumei butterfly. Nat. Nanotechnol. *5*, 511–515.

Kolle, M., Lethbridge, A., Kreysing, M., Baumberg, J.J., Aizenberg, J., and Vukusic, P. (2013). Bio-inspired band-gap tunable elastic optical multilayer fibers. Adv. Mater. *25*, 2239–2245.

Kristensen, A., Yang, J.K., Bozhevolnyi, S.I., Link, S., Nordlander, P., Halas, N.J., and Mortensen, N.A. (2016). Plasmonic colour generation. Nat. Rev. Mater. *2*, 1–14.

Kuang, M., Wang, J., Bao, B., Li, F., Wang, L., Jiang, L., and Song, Y. (2014a). Inkjet printing patterned photonic crystal domes for wide viewing-angle displays by controlling the sliding three phase contact line. Adv. Opt. Mater. *2*, 34–38.

Kuang, M., Wang, L., and Song, Y. (2014b). Controllable printing droplets for high-resolution patterns. Adv. Mater. *26*, 6950–6958.

Kulyk, O., Rocard, L., Maggini, L., and Bonifazi, D. (2020). Synthetic strategies tailoring colours in multichromophoric organic nanostructures. Chem. Soc. Rev.

Lee, T., Jang, J., Jeong, H., and Rho, J. (2018). Plasmonic-and dielectric-based structural coloring: from fundamentals to practical applications. Nano Convergence *5*, 1–21.

Li, Y., Zhou, X., Yang, Q., Li, Y., Li, W., Li, H., Chen, S., Li, M., and Song, Y. (2017). Patterned photonic crystals for hiding information. J. Mater. Chem. C *5*, 4621–4628.

Li, C., Zhao, M., Zhou, X., Li, H., Wang, Y., Hu, X., Li, M., Shi, L., and Song, Y. (2018). Janus structural color from a 2D photonic crystal hybrid with a fabry–perot cavity. Adv. Opt. Mater. *6*, 1800651.

Li, M., Lai, X., Li, C., and Song, Y. (2019a). Recent advantages of colloidal photonic crystals and their applications for luminescence enhancement. Mater. Today Nano *6*, 100039.

Li, W., Wang, Y., Li, M., Garbarini, L.P., and Omenetto, F.G. (2019b). Inkjet printing of patterned, multispectral, and biocompatible photonic crystals. Adv. Mater. *31*, 1901036.

Li, K., Zhang, T., Li, H., Li, M., and Song, Y. (2020). The precise assembly of nanoparticles. Acta Physico Chimica Sinica *36*, 52–70.

Liu, K., and Jiang, L. (2011). Bio-inspired design of multiscale structures for function integration. Nano Today *6*, 155–175.

Liu, Y., Wang, H., Ho, J., Ng, R.C., Ng, R.J., Hall-Chen, V.H., Koay, E.H., Dong, Z., Liu, H., and Qiu, C.-W. (2019). Structural color three-dimensional

printing by shrinking photonic crystals. Nat. Commun. *10*, 1–8.

Loewen, E.G., and Popov, E. (2018). Diffraction Gratings and Applications (CRC Press).

López, C. (2003). Materials aspects of photonic crystals. Adv. Mater. *15*, 1679–1704.

Mason, C.W. (2002). Structural colors in insects. II. J. Phys. Chem. A. *31*, 321–354.

McCoy, D.E., Feo, T., Harvey, T.A., and Prum, R.O. (2018). Structural absorption by barbule microstructures of super black bird of paradise feathers. Nat. Commun. *9*, 1–8.

Meyers, M.A., Chen, P.-Y., Lin, A.Y.-M., and Seki, Y. (2008). Biological materials: structure and mechanical properties. Prog. Mater. Sci. *53*, 1–206.

Min, L., Zhang, H., Pan, H., Wu, F., Hu, Y., Sheng, Z., Wang, M., Zhang, M., Wang, S., and Chen, X. (2019). Controllable liquid-liquid printing with defect-free, corrosion-resistance, unrestricted wetting condition. Iscience *19*, 93–100.

Moon, J.H., and Yang, S. (2010). Chemical aspects of three-dimensional photonic crystals. Chem. Rev. *110*, 547–574.

Morehouse, N.I., Vukusic, P., and Rutowski, R. (2007). Pterin pigment granules are responsible for both broadband light scattering and wavelength selective absorption in the wing scales of pierid butterflies. Proc. R. Soc. B Biol. Sci. *274*, 359–366.

Nam, H., Song, K., Ha, D., and Kim, T. (2016). Inkjet printing based mono-layered photonic crystal patterning for anti-counterfeiting structural colors. Sci. Rep. *6*, 30885.

Nussenzveig, H.M. (1969). High-Frequency scattering by a transparent sphere. I. direct reflection and transmission. J. Math. Phys. *10*, 82–124.

Pancharatnam, S. (1956). Generalized theory of interference and its applications. In Paper presented at: Proceedings of the Indian Academy of Sciences-Section A, *44* (Springer), pp. 398–417.

Phillips, K.R., Shirman, T., Shirman, E., Shneidman, A.V., Kay, T.M., and Aizenberg, J. (2018). Nanocrystalline precursors for the Co-assembly of crack-free metal oxide inverse opals. Adv. Mater. *30*, 1706329.

Qi, Y., Chu, L., Niu, W., Tang, B., Wu, S., Ma, W., and Zhang, S. (2019). New encryption strategy of photonic crystals with bilayer inverse heterostructure guided from transparency response. Adv. Funct. Mater. *29*, 1903743.

Ren, J., Wang, Y., Yao, Y., Wang, Y., Fei, X., Qi, P., Lin, S., Kaplan, D.L., Buehler, M.J., and Ling, S. (2019). Biological material interfaces as inspiration for mechanical and optical material designs. Chem. Rev. *119*, 12279–12336.

Richel, A., Johnson, N., and McComb, D. (2000). Observation of Bragg reflection in photonic crystals synthesized from air spheres in a titania matrix. Appl. Phys. Lett. *76*, 1816–1818.

Sanders, J. (1964). Colour of precious opal. Nature *204*, 1151–1153.

Shang, L., Zhang, W., Xu, K., and Zhao, Y. (2019). Bio-inspired intelligent structural color materials. Mater. Horizons *6*, 945–958.

Shi, L., Zhang, Y., Dong, B., Zhan, T., Liu, X., and Zi, J. (2013). Amorphous photonic crystals with only short-range order. Adv. Mater. *25*, 5314–5320.

Shin, H., Jo, S., and Mikos, A.G. (2003). Biomimetic materials for tissue engineering. Biomaterials *24*, 4353–4364.

Siddique, R.H., Donie, Y.J., Gomard, G., Yalamanchili, S., Merdzhanova, T., Lemmer, U., and Hölscher, H. (2017). Bioinspired phase-separated disordered nanostructures for thin photovoltaic absorbers. Sci. Adv. *3*, e1700232.

Skipetrov, S.E., and Sokolov, I.M. (2014). Absence of Anderson localization of light in a random ensemble of point scatterers. Phys. Rev. Lett. *112*, 023905.

Sköld, K., Rowe, J., Ostrowski, G., and Randolph, P. (1972). Coherent-and incoherent-scattering laws of liquid argon. Phys. Rev. A. *6*, 1107.

Sun, J., Bhushan, B., and Tong, J. (2013). Structural coloration in nature. RSC Adv. *3*, 14862–14889.

Syurik, J., Jacucci, G., Onelli, O.D., Hölscher, H., and Vignolini, S. (2018). Bio-inspired highly scattering networks via polymer phase separation. Adv. Funct. Mater. *28*, 1706901.

Tadepalli, S., Slocik, J.M., Gupta, M.K., Naik, R.R., and Singamaneni, S. (2017). Bio-optics and bio-inspired optical materials. Chem. Rev. *117*, 12705–12763.

Tan, A.T., Beroz, J., Kolle, M., and Hart, A.J. (2018). Direct-write freeform colloidal assembly. Adv. Mater. *30*, 1803620.

Tan, H., Lyu, Q., Xie, Z., Li, M., Wang, K., Wang, K., Xiong, B., Zhang, L., and Zhu, J. (2019). Metallosupramolecular photonic elastomers with self-healing capability and angle-independent color. Adv. Mater. *31*, 1805496.

Teyssier, J., Saenko, S.V., Van Der Marel, D., and Milinkovitch, M.C. (2015). Photonic crystals cause active colour change in chameleons. Nat. Commun. *6*, 1–7.

Tian, E., Wang, J., Zheng, Y., Song, Y., Jiang, L., and Zhu, D. (2008). Colorful humidity sensitive photonic crystal hydrogel. J. Mater. Chem. C *18*, 1116–1122.

Vogel, N., Retsch, M., Fustin, C.-A., del Campo, A., and Jonas, U. (2015a). Advances in colloidal assembly: the design of structure and hierarchy in two and three dimensions. Chem. Rev. *115*, 6265–6311.

Vogel, N., Utech, S., England, G.T., Shirman, T., Phillips, K.R., Koay, N., Burgess, I.B., Kolle, M., Weitz, D.A., and Aizenberg, J. (2015b). Color from hierarchy: diverse optical properties of micron-sized spherical colloidal assemblies. Proc. Natl. Acad. Sci. U S A *112*, 10845–10850.

Vukusic, P., and Sambles, J.R. (2003). Photonic structures in biology. Nature *424*, 852–855.

Wang, H., and Zhang, K.-Q. (2013). Photonic crystal structures with tunable structure color as colorimetric sensors. Sensors *13*, 4192–4213.

Wang, L., Wang, K., Santra, S., Zhao, X., Hilliard, L.R., Smith, J.E., Wu, Y., and Tan, W. (2006). Watching Silica Nanoparticles Glow in the Biological World (ACS Publications).

Wang, M., He, L., Xu, W., Wang, X., and Yin, Y. (2015). Magnetic assembly and field-tuning of ellipsoidal-nanoparticle-based colloidal photonic crystals. Angew. Chem.-Int. Edit. *54*, 7077–7081.

Wang, Y., Cui, H., Zhao, Q., and Du, X. (2019a). Chameleon-inspired Structural-color Actuators. Matter *1*, 626–638.

Wang, H., Liu, Y., Chen, Z., Sun, L., and Zhao, Y. (2020). Anisotropic structural color particles from colloidal phase separation. Sci. Adv. *6*, eaay1438.

Watanabe, K., Hoshino, T., Kanda, K., Haruyama, Y., and Matsui, S. (2004). Brilliant blue observation from a Morpho-butterfly-scale quasi-structure. Jpn. J. Appl. Phys. *44*, L48.

Whitney, H.M., Kolle, M., Andrew, P., Chittka, L., Steiner, U., and Glover, B.J. (2009). Floral iridescence, produced by diffractive optics, acts as a cue for animal pollinators. Science *323*, 130–133.

Wilts, B.D., Sheng, X., Holler, M., Diaz, A., Guizar-Sicairos, M., Raabe, J., Hoppe, R., Liu, S.H., Langford, R., and Onelli, O.D. (2018). Evolutionary-optimized photonic network structure in white beetle wing scales. Adv. Mater. *30*, 1702057.

Wu, L., Dong, Z., Kuang, M., Li, Y., Li, F., Jiang, L., and Song, Y. (2015). Printing patterned fine 3D structures by manipulating the three phase contact line. Adv. Funct. Mater. *25*, 2237–2242.

Wu, P., Wang, J., and Jiang, L. (2020). Bio-inspired photonic crystal patterns. Mater. Horizons *7*, 338–365.

Xiao, M., Li, Y., Allen, M.C., Deheyn, D.D., Yue, X., Zhao, J., Gianneschi, N.C., Shawkey, M.D., and Dhinojwala, A. (2015). Bio-inspired structural colors produced via self-assembly of synthetic melanin nanoparticles. ACS Nano *9*, 5454–5460.

Xiao, M., Hu, Z., Wang, Z., Li, Y., Tormo, A.D., Le Thomas, N., Wang, B., Gianneschi, N.C., Shawkey, M.D., and Dhinojwala, A. (2017). Bioinspired bright noniridescent photonic melanin supraballs. Sci. Adv. *3*, e1701151.

Yang, X.-Y., Chen, L.-H., Li, Y., Rooke, J.C., Sanchez, C., and Su, B.-L. (2017). Hierarchically porous materials: synthesis strategies and structure design. Chem. Soc. Rev. *46*, 481–558.

Yang, B., Cai, F., Huang, S., and Yu, H. (2020). Athermal and soft multi-nanopatterning of azopolymers: phototunable mechanical properties. Angew. Chem. *132*, 4064–4071.

Yeo, S.J., Park, K.J., Guo, K., Yoo, P.J., and Lee, S. (2016). Microfluidic generation of monodisperse and photoreconfigurable microspheres for floral iridescence–inspired structural colorization. Adv. Mater. *28*, 5268–5275.

Young, A.T. (1981). Rayleigh scattering. Appl. Opt. *20*, 533–535.

Yu, Z., Wang, C.F., Ling, L., Chen, L., and Chen, S. (2012). Triphase microfluidic-directed self-assembly: anisotropic colloidal photonic crystal supraparticles and multicolor patterns made easy. Angew. Chem. *124*, 2425–2428.

Zhang, C., Mcadams, D.A., and Grunlan, J.C. (2016). Nano/micro-manufacturing of bioinspired materials: a review of methods to mimic natural structures. Adv. Mater. *28*, 6292–6321.

Zhang, Y., Han, P., Zhou, H., Wu, N., Wei, Y., Yao, X., Zhou, J., and Song, Y. (2018). Highly brilliant noniridescent structural colors enabled by graphene nanosheets containing graphene quantum dots. Adv. Funct. Mater. *28*, 1802585.

Zhang, J., Meng, Z., Liu, J., Chen, S., and Yu, Z. (2019a). Spherical colloidal photonic crystals with selected lattice plane exposure and enhanced color saturation for dynamic optical displays. ACS Appl. Mater. Inter. *11*, 42629–42634.

Zhang, J., Zhu, Z., Yu, Z., Ling, L., Wang, C.-F., and Chen, S. (2019b). Large-scale colloidal films with robust structural colors. Mater. Horizons *6*, 90–96.

Zhao, X., Cao, Y., Ito, F., Chen, H.H., Nagai, K., Zhao, Y.H., and Gu, Z.Z. (2006). Colloidal crystal beads as supports for biomolecular screening. Angew. Chem. Int. Edit. *45*, 6835–6838.

Zhao, Y., Zhao, X., Hu, J., Xu, M., Zhao, W., Sun, L., Zhu, C., Xu, H., and Gu, Z. (2009). Encoded porous beads for label-free multiplex detection of tumor markers. Adv. Mater. *21*, 569–572.

Zhao, Y., Xie, Z., Gu, H., Zhu, C., and Gu, Z. (2012). Bio-inspired variable structural color materials. Chem. Soc. Rev. *41*, 3297.

Zhao, Y., Gu, H., Xie, Z., Shum, H.C., Wang, B., and Gu, Z. (2013). Bioinspired multifunctional Janus particles for droplet manipulation. J. Am. Chem. Soc. *135*, 54–57.

Zhao, Y., Shang, L., Cheng, Y., and Gu, Z. (2014). Spherical colloidal photonic crystals. Acc. Chem. Res. *47*, 3632–3642.

Zhao, Q., Finlayson, C.E., Snoswell, D.R., Haines, A., Schäfer, C., Spahn, P., Hellmann, G.P., Petukhov, A.V., Herrmann, L., and Burdet, P. (2016). Large-scale ordering of nanoparticles using viscoelastic shear processing. Nat. Commun. *7*, 1–10.

Zhao, C., Li, H., Wang, Y., Li, K., Hou, J., Ma, Y., Li, M., and Song, Y. (2019). A general layer-by-layer printing method for scalable high-resolution full-color flexible luminescent patterns. Adv. Opt. Mater. *7*, 1900127.

Zhao, T.H., Jacucci, G., Chen, X., Song, D.P., Vignolini, S., and Parker, R.M. (2020). Angular-independent photonic pigments via the controlled micellization of amphiphilic bottlebrush block copolymers. Adv. Mater. *32*, e2002681.

Zhong, K., Li, J., Liu, L., Van Cleuvenbergen, S., Song, K., and Clays, K. (2018). Instantaneous, simple, and reversible revealing of invisible patterns encrypted in robust hollow sphere colloidal photonic crystals. Adv. Mater. *30*, 1707246.

Zhou, Z., and Zhao, X. (2005). Opal and inverse opal fabricated with a flow-controlled vertical deposition method. Langmuir *21*, 4717–4723.

Zhou, Q., Park, J.G., Bae, J., Ha, D., Park, J., Song, K., and Kim, T. (2020). Multimodal and covert–overt convertible structural coloration transformed by mechanical stress. Adv. Mater. *32*, e2001467.

Zhu, S., Yu, A., Hawley, D., and Roy, R. (1986). Frustrated total internal reflection: a demonstration and review. Am. J. Phys. *54*, 601–607.

Zi, J., Yu, X., Li, Y., Hu, X., Xu, C., Wang, X., Liu, X., and Fu, R. (2003). Coloration strategies in peacock feathers. Proc. Natl. Acad. Sci. U S A *100*, 12576–12578.